

AD-A050 267

AUBURN UNIV ALA DEPT OF AEROSPACE ENGINEERING
ANALYSIS AND COMPARISON OF SEVERAL METHODS FOR COMPUTING AERODY--ETC(U)
SEP 77 F W MARTIN, J PURVIS, J E BURKHALTER F08635-77- C-0002
AFATL-TR-77-112 NL

UNCLASSIFIED

| OF |
AD
A050267



END
DATE
FILMED
3-78
DDC

AD A 050267

2
B.S.

AFATL-TR-77-112



**ANALYSIS AND COMPARISON OF SEVERAL
METHODS FOR COMPUTING AERODYNAMIC
COMPRESSIBILITY AND INTERFERENCE EFFECTS
UP TO CRITICAL MACH NUMBERS**

DEPT. OF AEROSPACE ENGINEERING
AUBURN UNIVERSITY
AUBURN, ALABAMA 36830

SEPTEMBER 1977

FINAL REPORT FOR PERIOD
OCTOBER 1976 TO SEPTEMBER 1977

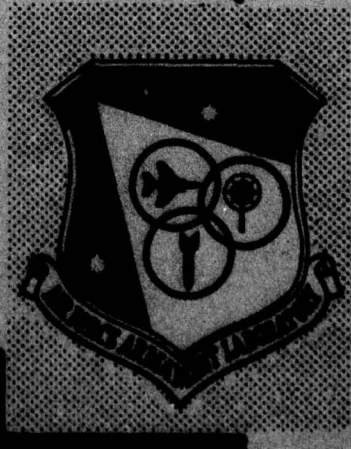
DDC
RECEIVED
FEB 21 1978
RECEIVED
Q1 D

Approved for public release; distribution unlimited

AIR FORCE ARMAMENT LABORATORY

AIR FORCE SYSTEMS COMMAND • UNITED STATES AIR FORCE

EGLIN AIR FORCE BASE, FLORIDA



AU NO. _____
DDC FILE COPY

39 REPORT DOCUMENTATION PAGE		READ INSTRUCTIONS BEFORE COMPLETING FORM	
1. REPORT NUMBER	2. GOVT ACCESSION NO.	3. RECIPIENT'S CATALOG NUMBER	
18 AFATL-TR-77-112			
4. TITLE (and Subtitle)		5. TYPE OF REPORT & PERIOD COVERED	
6 ANALYSIS AND COMPARISON OF SEVERAL METHODS FOR COMPUTING AERODYNAMIC COMPRESSIBILITY AND INTERFERENCE EFFECTS UP TO CRITICAL MACH NUMBERS		9 Final Report, Oct 1976 - Sep 1977	
7. AUTHOR(s)		6. PERFORMING ORG. REPORT NUMBER	
10 Fred W. Martin, John E. Burkhalter James Purvis, Brent D. Martin		8. CONTRACT OR GRANT NUMBER(s)	
		15 F08635-77-C-0002	
9. PERFORMING ORGANIZATION NAME AND ADDRESS		10. PROGRAM ELEMENT, PROJECT, TASK AREA & WORK UNIT NUMBERS	
Department of Aerospace Engineering Auburn University Auburn, Alabama 36830		17 JON 2567-02-15 Program Element 62602F	
11. CONTROLLING OFFICE NAME AND ADDRESS		12. REPORT DATE	
Air Force Armament Laboratory Armament Development and Test Center Eglin AFB, Florida 32542		11 Sept 1977	
14. MONITORING AGENCY NAME & ADDRESS (if different from Controlling Office)		13. NUMBER OF PAGES	
		62 12 62 p.	
		15. SECURITY CLASS. (of this report)	
		Unclassified	
		15a. DECLASSIFICATION/DOWNGRADING SCHEDULE	
16. DISTRIBUTION STATEMENT (of this Report)			
Approved for public release; distribution unlimited			
17. DISTRIBUTION STATEMENT (of the abstract entered in Block 20, if different from Report)			
18. SUPPLEMENTARY NOTES			
Available in DDC.			
19. KEY WORDS (Continue on reverse side if necessary and identify by block number)			
Aerodynamic analysis Small disturbance potential analysis Exact potential analysis Pressure distribution			
20. ABSTRACT (Continue on reverse side if necessary and identify by block number)			
Analytical approaches are considered which might be used to improve and extend current aerodynamic analysis to include the compressibility effects up to and including critical mach numbers. The Rayleigh-Janzen solution is considered for both small disturbance and exact potential flows. A simple numerical method is presented and compared with both experimental results and the results of other analytical methods for potential flow.			

PREFACE

The work effort reported herein represents an attempt to upgrade the analytical solutions developed as part of a continuing technical effort under contract numbers F08635-71-C-0090, F08635-75-C-0023, and F08635-76-C-0079. This effort is the result of the work done during the period from October 1976 to September 1977 by the Department of Aerospace Engineering, Auburn University, Auburn, Alabama 36830, under contract number F08635-77-C-0002 with the Air Force Armament Laboratory, Armament Development and Test Center, Eglin Air Force Base, Florida 32542. Program manager was Captain Robert A. Grow (DLJCA). This report constitutes the final report for this contract.

This report has been reviewed by the Information Officer (OI) and is releasable to the National Technical Information Service (NTIS). At NTIS, it will be available to the general public, including foreign nations.

This technical report has been reviewed and is approved for publication.

FOR THE COMMANDER:

William F. Brockman
WILLIAM F. BROCKMAN, Colonel, USAF
Chief, Munitions Division

ACCESSION FOR	
NTIS	White Section <input checked="" type="checkbox"/>
DDP	Buff Section <input type="checkbox"/>
UNANNOUNCED	<input type="checkbox"/>
JUSTIFICATION	
BY	
DISTRIBUTION/AVAILABILITY CODES	
Dist.	AVAIL. and/or SPECIAL
A	

D D C
RECEIVED
FEB 21 1978
RECEIVED
D

TABLE OF CONTENTS

Section	Title	Page
I	INTRODUCTION	1
II	APPROXIMATE SOLUTIONS.	3
	Introduction.	3
	Slender Body Solution	3
	Modified Slender Body Solution.	5
	Successive Numerical Approximation.	12
III	EXACT NUMERICAL SOLUTION, PURVIS METHOD.	15
	Introduction.	15
	Governing Equation.	16
	Divergence Integral	16
	General Solution.	16
	Cell Formulation.	17
	Body Boundary Conditions.	19
	Stretched Coordinates	19
	Initial Conditions.	20
	Comparison with Experiment.	20
	Computational Parameters.	24
	Comparison with Other Methods	26
	Conclusions	26
	Recommendations	26
IV	DISCUSSION OF BOUNDARY LAYER STUDY	29

TABLE OF CONTENTS (CONCLUDED)

Section	Title	Page
	Introduction	29
	Mathematical Approach.	29
	Conclusions.	32
V	DISCUSSION OF FINITE ELEMENTS STUDY	33
	Introduction	33
	Governing Equations.	34
	Solution Procedure	34
	Finite Element Formulation	34
VI	SUMMARY OF RESULTS WITH COMMENTS AND RECOMMENDATIONS. .	42
	Summary of Results with Comments	42
	Recommendations.	43
Appendix		
A	RAYLEIGH-JANZEN SOLUTION.	45
B	MODIFIED SLENDER BODY SOLUTION.	52
	REFERENCES	55

LIST OF FIGURES

Figure	Title	Page
1.	Comparison of Theoretical Results and Experiment Showing the Effects of the Order of Magnitude Solutions	6
2.	Comparison of Theoretical and Experimental Pressure Distributions for Several Mach Numbers, $\alpha=0^\circ$	7
3.	Comparison of Rayleigh-Janzen Solution and Solution Using Gothert's Rule, M117 Bomb Shape, $\alpha=0^\circ$, $M_\infty=0.8$	10
4.	Comparison of Rayleigh-Janzen Solution and Solution Using Gothert's Rule with Maximum Volume Bombs Shape, $\alpha=0^\circ$, $M_\infty=0.5$	11
5.	Schematic of Computational Cell	18
6.	Schematic of Body Boundary Cell	18
7.	Comparison of Numerical Solution Using Purvis Method and Experiment for a 6 Percent Parabolic Arc Airfoil.	21
8.	Comparison of Numerical Solution Using Purvis Method and Experiment for Double Wedge Airfoil	22
9.	Comparison of Numerical Solution Using Purvis Method and Experiment for an M117 Bomb Shape	23
10.	Comparison of Numerical Solution Using Purvis Method and Experiment for 16-Inch Maximum Volume Hemispherical Nose Bomb.	25
11.	Axisymmetric Body with a Curved Boundary Layer Plane.	30
12.	Schematic of Body Boundary Condition Coordinates for Finite Element Analysis	36
13.	Schematic of Finite Elements Showing Numbering Scheme	38
14.	Comparison of the Pressure Distributions for a 6 Percent Parabolic Arc Airfoil, Computed by the Finite Element Method with Experimental Results, $M_\infty=0.707$	41

SECTION I

INTRODUCTION

During the past several years the authors have generated analytical techniques for predicting the mutual aerodynamic interference between externally carried stores and between the stores and the aircraft (References 1 through 10). Although some solution techniques using surface singularities are considered, the basic approach utilizes the Rankine method of superposition of an axial source-sink distribution to form a closed body. The interference flow fields are then superimposed on the isolated solutions for the external stores (finned bodies of revolution) and the aircraft components (fuselage, wing, and pylon).

The work previously performed in this general area has been limited to solutions of the Prandtl-Glauert equation, a form of the governing differential equation which was linearized by assuming inviscid fluid, small velocity perturbations, and avoiding the transonic regime. Comparison of this analytical work with wind tunnel test data has shown, however, that the linearized solutions will not predict accurately the compressible flow effects at conditions approaching the critical mach number. Further, in the case of the triple ejector rack (TER) with stores, the pressures observed experimentally are indicative of large velocity perturbations, i.e., near stagnation values forward of the bomb rack. It is felt, therefore, that both transonic and large perturbation terms will have to be considered.

In addition to the large velocity perturbation and transonic terms, it is very likely that the viscous effects will have to be included in order to predict the loading for some configurations. This is particularly true in the case of multiple weapons carriage such as with TERs and multiple ejector racks (MERs). For example, in the case of three M117 bombs on a TER, the boundary layers between bombs coalesce. Thus, the usual simple boundary layer displacement corrections cannot be used. Also, in the case of a shockwave-boundary layer interaction, the solutions for the boundary layer and the potential flow are mutually dependent; therefore, the significant terms in the governing differential equations are nonlinear.

While it is quite desirable to obtain a solution which includes all of the nonlinear terms, more restrictive approaches are generally more fruitful. Because of this, several approximate as well as exact approaches were simultaneously pursued in this effort.

At the time that this effort was initiated, it was felt that the approach most likely to succeed for the inviscid flow case would be to

generate higher order effects based on the current image-system solution. Basically, the approach would be to evaluate the effects of the nonlinear terms which previously have been neglected from the governing differential equation for inviscid flow. This would be done by the successive approximation technique or by the more orderly method of asymptotic expansion. Considerable effort was put into this approach, and the results are discussed in this report.

Initially it was felt that the best approach for the viscous flow problem would be to use the current potential flow solution (see References 1 through 10) for the far-field boundary conditions and use an imbedded numerical solution technique for the boundary layer and boundary layer-shock wave solutions. This concept was pursued using classical numerical marching techniques. It became evident, however, that a more general numerical solution is required.

In addition, other numerical approaches have been studied which, along with the efforts mentioned above, are discussed in detail in the following sections of this report.

SECTION II

APPROXIMATE SOLUTIONS

INTRODUCTION

The current solutions given in References 1 through 10 are limited to the case of slender bodies for which the flow is all either subsonic or supersonic. Specifically, this previous work represents solutions to the Prandtl-Glauert equation which is the linearized velocity potential equation given as Equation (1).

$$(1-M_\infty^2)\phi_{xx} + \phi_{yy} + \phi_{zz} = 0 \quad (1)$$

Noting that Equation (1) becomes the Laplace equation if the free stream mach number is zero, it is seen that for this case the restriction of small velocity perturbations can be removed. This is the so-called zeroth solution and can be used as a basis for generating the compressibility effects at higher mach numbers by a successive approximation technique, or by the more orderly method of assuming a solution in the form of a series. A classical series solution known as the Rayleigh-Janzen method has been used in a nearly exact manner for a few simple problems as noted by Shapiro (Reference 11). Although this type of solution technique has been greatly extended (see Reference 12) by other investigators, it has been applied only to simple isolated bodies. It was felt, however, that because of the current, closed form, analytical solutions for aerodynamic interference (see References 1 through 10) the Rayleigh-Janzen method could be used for this problem. In order to verify this approach, several formulations of the solution were generated for an isolated slender body as follows:

SLENDER BODY SOLUTION

The usual form of the velocity potential equation is written as follows (for two dimensions):

$$(\phi_x^2 - a^2)\phi_{xx} + 2\phi_x\phi_y\phi_{xy} + (\phi_y^2 - a^2)\phi_{yy} = 0 \quad (2)$$

where a is the sonic speed and can be expressed as

$$a^2 = a_\infty^2 \left[1 + \left(\frac{\gamma-1}{2}\right) M_\infty^2 (V_\infty^2 - \phi_x^2 - \phi_y^2) \right] \quad (3)$$

Equation (2) is the form of the velocity potential equation usually found in the literature as the most general form (for two-dimensions). For this study, however, it was found that a more useful form is given by Equation (4) or its equivalent Equation (5).

$$a^2 \nabla^2 \phi = - \left(\frac{1}{\gamma-1} \right) \nabla \phi \cdot \nabla a^2 \quad (4)$$

or

$$\nabla^2 \phi = - \left(\frac{1}{\gamma-1} \right) \nabla \phi \cdot \nabla \ln a^2 \quad (5)$$

which hold for both two- and three-dimensional cases.

Expanding Equation (4) in terms of the perturbation velocity potential yields a nondimensional form (3 dimensions):

$$\begin{aligned} [1 - \left(\frac{\gamma-1}{2} \right) M_\infty^2 (2\phi_x + \phi_x^2 + \phi_y^2 + \phi_z^2)] \nabla^2 \phi = \\ \frac{M_\infty^2}{2} [(\phi_x + 1) \frac{\partial}{\partial x} + \phi_y \frac{\partial}{\partial y} + \phi_z \frac{\partial}{\partial z}] (2\phi_x + \phi_x^2 + \phi_y^2 + \phi_z^2) \end{aligned} \quad (6)$$

Since we are looking for the compressibility effects, we can set $\epsilon = M_\infty^2$, where ϵ will be our perturbation parameter, and assume a solution of the form

$$\phi(x,y,z;\epsilon) = \phi^{(0)}(x,y,z) + \epsilon \phi^{(1)}(x,y,z) + \epsilon^2 \phi^{(2)}(x,y,z) + \dots \quad (7)$$

The assumed solution can be substituted in Equation (6) and (in principle) each successive order of magnitude term can be solved. For small perturbations, however, Equation (6) can be simplified by neglecting velocity-squared terms in comparison to first-order terms and after some manipulation reduces to

$$[1 - (\gamma-1) M_\infty^2 \phi_x] a^2 \nabla^2 \phi = M_\infty^2 \phi_{xx} \quad (8)$$

For slender axisymmetric bodies at zero angle of attack the body boundary conditions can be expressed as

$$\phi_y \cos \theta + \phi_z \sin \theta = (1 + \phi_x) \frac{dr}{dx} \Big|_{\text{body}} \quad (9)$$

Substituting Equation (7) into Equations (8) and (9), and equating terms in powers of ϵ gives a set of order of magnitude equations. The first three, zeroth, first, and second orders, are given in Appendix A.

The numerical results of applying this solution to an M117 bomb shape are presented as Figures 1 and 2. On Figure 1, the theoretical results through the second-order terms are compared with the wind tunnel test results of Reference 13. Figure 2 shows a comparison with experiment for the second-order solution; there is very good agreement for mach numbers 0.5 and 0.8. At mach number 0.8, however, the critical free stream mach number has been exceeded as evidenced by a slight jump in the pressure distribution at an axial station of about $X/D = 1.5$. A much larger pressure jump can be seen for the mach number case of $M = 0.9$. The pressure on the nose of the body is predicted quite well, however, up to a value of $X/D = 1.0$ where the local flow has become supersonic.

In principle, this solution can be applied to the multibody interference solution as outlined in References 3, 6, 8, and 9. In the case of three large bombs mounted on a triple ejector rack, however, there will be nearly stagnation pressures in the vicinity of the bomb racks, and, therefore, the small perturbation assumption will be violated.

It was felt that a more exact solution would be needed in order to obtain a valid solution in the vicinity of stagnation points; therefore, a modified slender body solution has been formulated.

MODIFIED SLENDER BODY SOLUTION

A convenient form of the differential equation which is valid at stagnation points can be obtained by using Equation(5) which, written in terms of the non-dimensional perturbation velocity potential, becomes

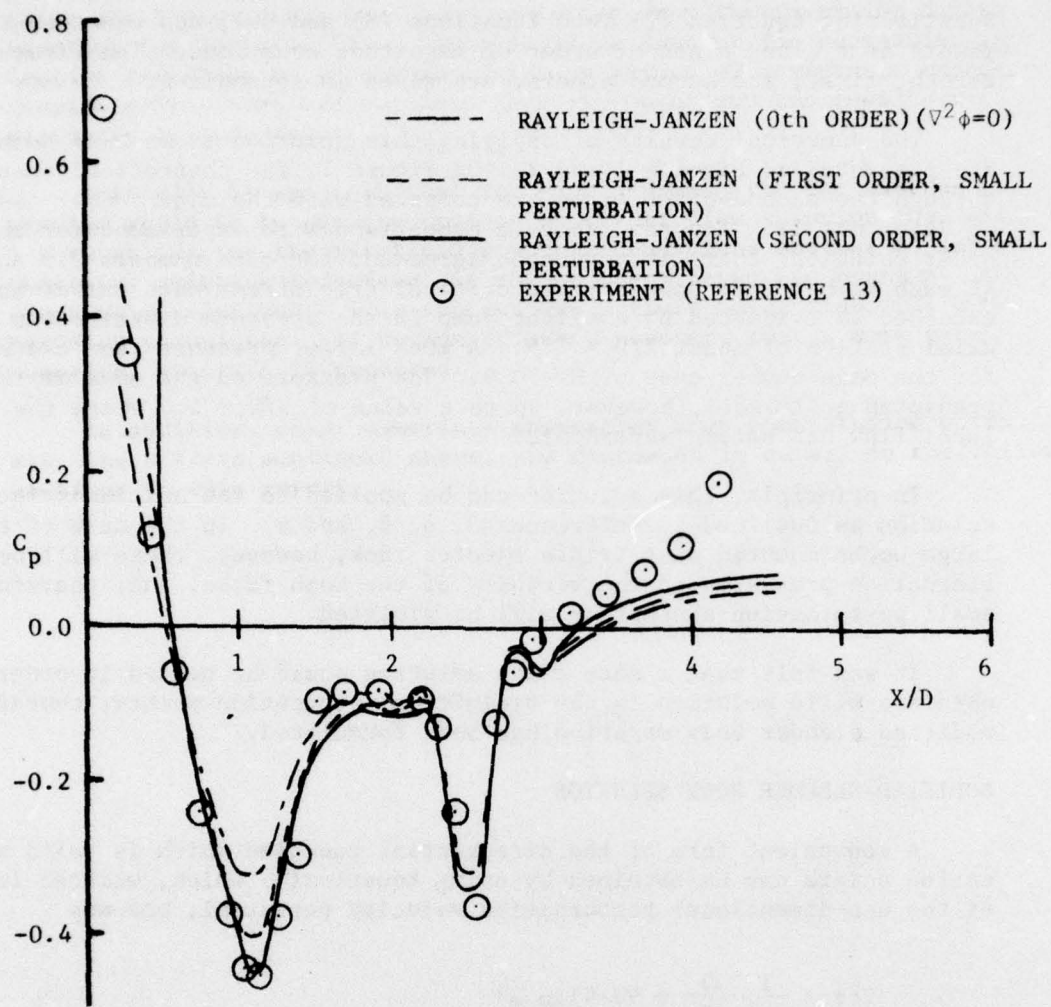
$$\nabla^2 \phi = \frac{1}{\gamma-1} \left(\frac{\partial}{\partial x} + \nabla \phi \cdot \nabla \right) \ln a^2 \quad (10)$$

where a^2 is the square of the nondimensional speed of sound and in terms of the perturbation potential function can be expressed as

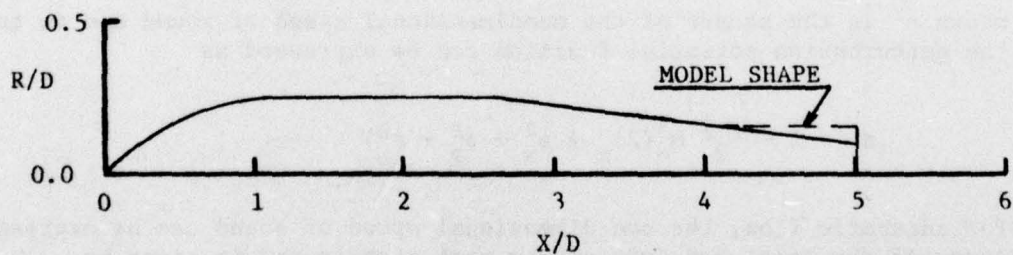
$$a^2 = 1 - \frac{\gamma-1}{2} M_\infty^2 (2\phi_x + \phi_x^2 + \phi_y^2 + \phi_z^2) \quad (11)$$

For adiabatic flow, the non-dimensional speed of sound can be expressed in terms of the local and free stream mach numbers and is given by

$$a^2 = \frac{1 + \frac{\gamma-1}{2} M^2}{1 + \frac{\gamma-1}{2} M_\infty^2} \quad (12)$$



(A). $M_\infty = 0.8$



(B). M117 Profile

Figure 1. Comparison of Theoretical Results and Experiment Showing the Effects of the Order of Magnitude Solutions

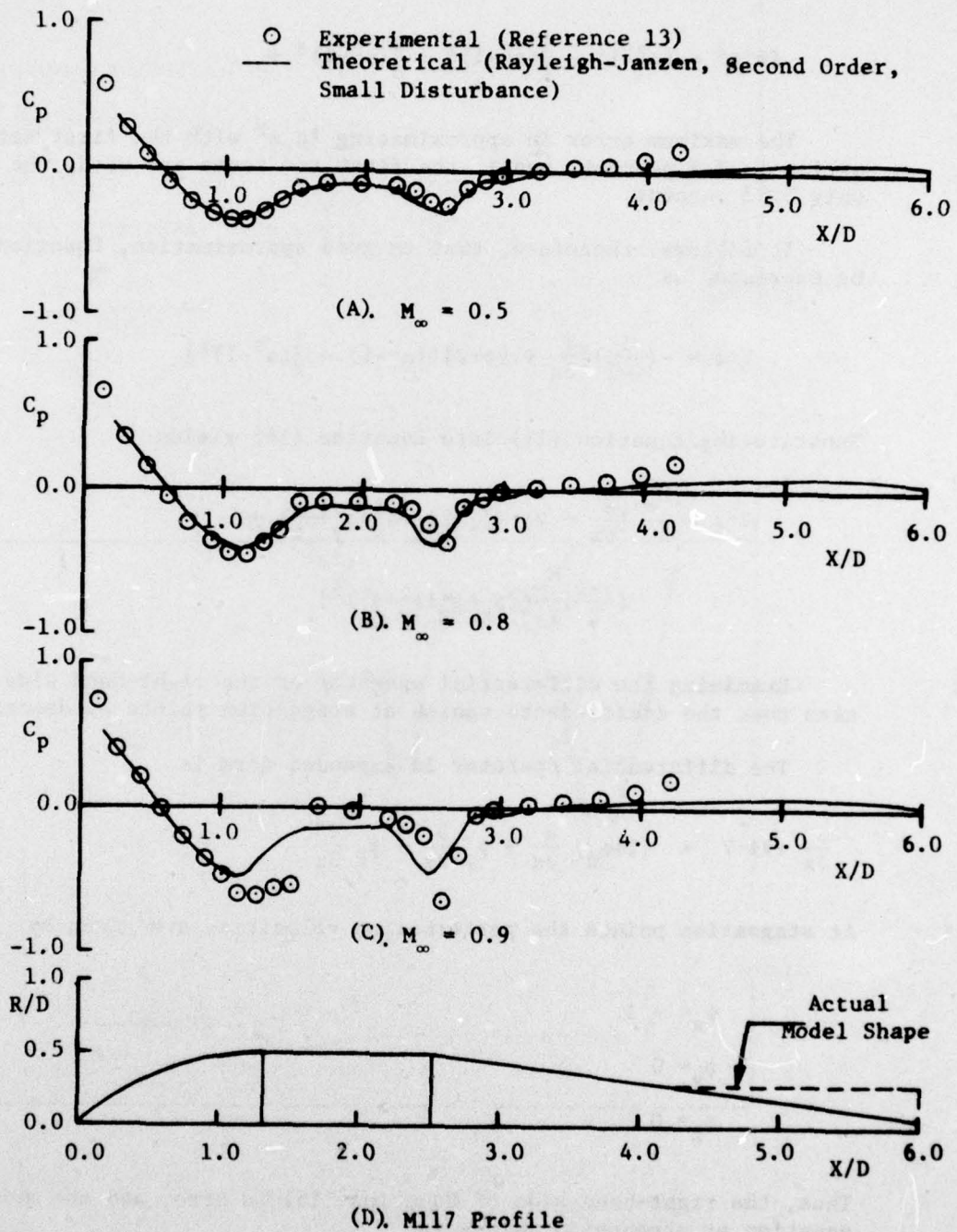


Figure 2. Comparison of Theoretical and Experimental Pressure Distributions for Several Mach numbers, $\alpha=0^\circ$

From this expression it can be seen that the minimum value of a^2 for sub-critical speeds is given for $M=0$ and $M_\infty=1$. This gives a value of $a^2=0.8333$. Thus, an appropriate expansion for $\ln a^2$ is given by the series,

$$\ln a^2 = (a^2-1) - \frac{1}{2}(a^2-1)^2 + \frac{1}{3}(a^2-1)^3 + \dots \quad (13)$$

The maximum error in approximating $\ln a^2$ with the first term of the series is 8.5 percent, and if the first two terms are used, the error is only 0.82 percent.

It follows, therefore, that to good approximation, Equation (10) can be expressed as

$$\nabla^2 \phi = -\left(\frac{1}{\gamma-1}\right) \left[\frac{\partial}{\partial x} + \nabla \phi \cdot \nabla \right] \left[(a^2-1) - \frac{1}{2}(a^2-1)^2 \right] \quad (14)$$

Substituting Equation (11) into Equation (14) yields

$$\begin{aligned} \nabla^2 \phi = \frac{M_\infty^2}{2} \left[\frac{\partial}{\partial x} + \nabla \phi \cdot \nabla \right] \left[(2\phi_x + \phi_x^2 + \phi_y^2 + \phi_z^2) + \right. \\ \left. \left(\frac{\gamma-1}{2}\right) \frac{M_\infty}{2} (2\phi_x + \phi_x^2 + \phi_y^2 + \phi_z^2)^2 \right] \quad (15) \end{aligned}$$

Examining the differential operator on the right-hand side, it can be seen that the coefficients vanish at stagnation points as described below:

The differential operator in expanded form is

$$\frac{\partial}{\partial x} + \nabla \phi \cdot \nabla = (1+\phi_x) \frac{\partial}{\partial x} + \phi_y \frac{\partial}{\partial y} + \phi_z \frac{\partial}{\partial z} \quad (16)$$

At stagnation points the perturbation velocities are given by

$$\begin{aligned} \phi_x &= -1 \\ \phi_y &= 0 \\ \phi_z &= 0 \end{aligned} \quad (17)$$

Thus, the right-hand side of Equation (15) is zero, and the governing equation at stagnation points is

$$\nabla^2 \phi = 0 \quad (18)$$

NOTE: Equation (18) holds at stagnation points whether the term, $\ln a^2$, is or is not approximated with the truncated series.

It follows that the term on the right-hand side of Equation (15) has negligible effect in the vicinity of stagnation points.

Now, if it is assumed that the velocity perturbations are small at points away from stagnation conditions, it can be assumed that

$$\phi_x^2 + \phi_y^2 + \phi_z^2 \ll 2\phi_x \quad (19)$$

To good approximation, therefore, Equation (15) can be expressed as

$$\nabla^2 \phi = \left[\frac{\partial}{\partial x} + \nabla \phi \cdot \nabla \right] \left[M_\infty^2 \phi_x + \left(\frac{\gamma-1}{2} \right) M_\infty^4 \phi_x^2 \right] \quad (20)$$

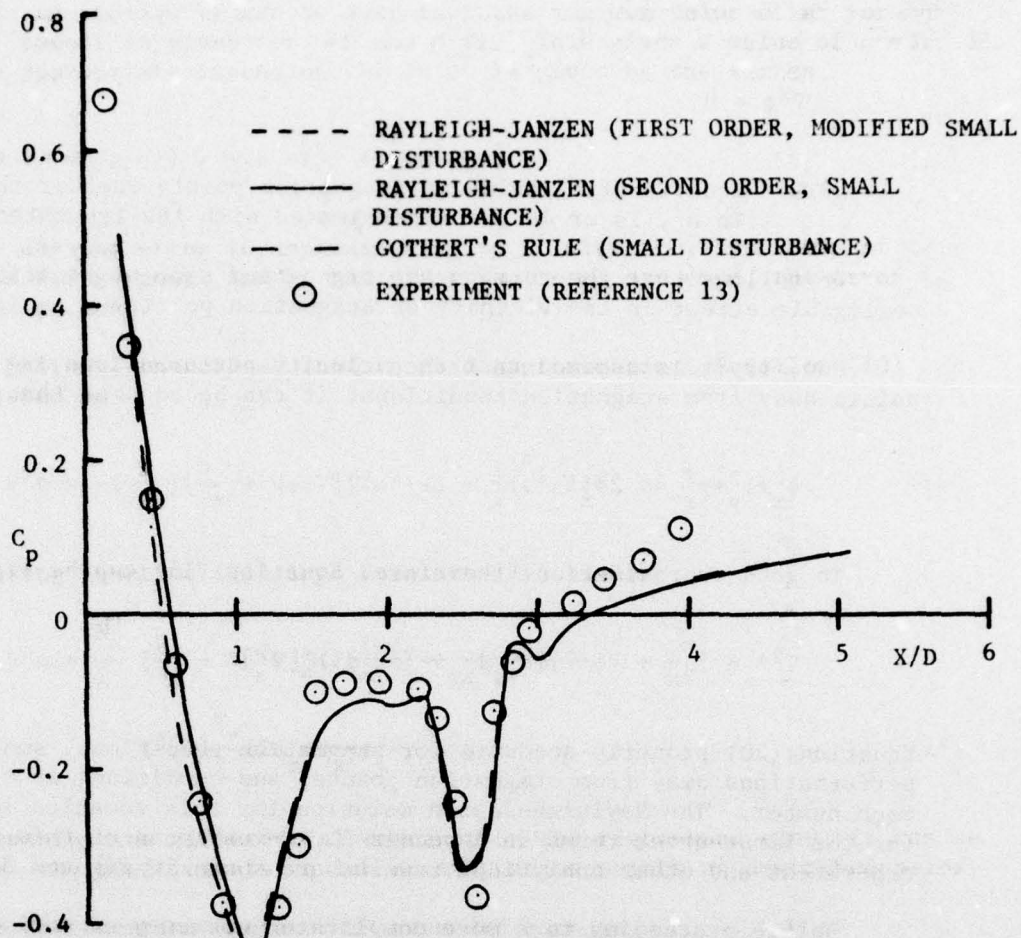
Equation (20) properly accounts for stagnation conditions, small velocity perturbations away from stagnation points, and conditions up to the critical mach number. The Rayleigh-Janzen solution for this equation is developed for the first-order terms in Appendix B. Comparisons of this result with experiment and other analytical results are shown in Figures 3 and 4.

Before proceeding to a more complicated geometry or analysis, however, it is of interest to note the following:

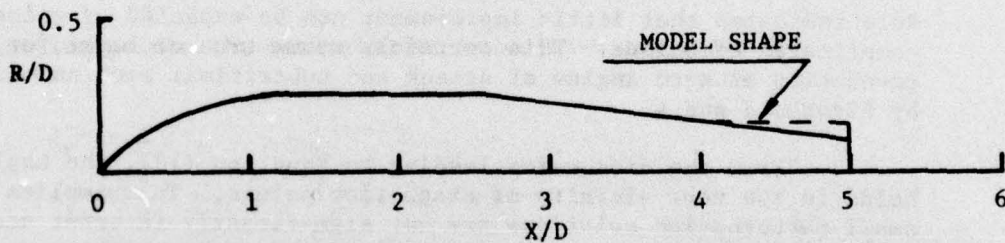
1. Comparison of the Rayleigh-Janzen results (this analysis, both slender body and modified slender body) with the solution using Gothert's Rule indicates that little improvement can be expected by going to this more complicated technique. This certainly seems true at least for bodies of revolution at zero angles of attack and subcritical mach numbers as indicated by Figures 3 and 4.

2. From the discussion leading to Equation (18), the Laplace equation holds in the near vicinity of stagnation points. This implies that the small perturbation solutions are not significantly in error near stagnation points. This conclusion is borne out by the agreement between the theories and experiments shown on Figures 1 through 4.

3. The analytical approaches discussed above are valid only for pure subsonic flow. This can be seen on Figure 2. There is only a slight jump in the experimental pressure coefficient at $M_\infty=0.8$, but at $M_\infty=0.9$, this jump is quite prominent. In fact, the discrepancy between the analytical and experimental pressure coefficients is quite large for the $M_\infty=0.9$ case.



(A). Pressure Distribution $M_\infty = 0.8$



(B). Schematic of Body Profile

Figure 3. Comparison of Rayleigh-Janzen Solution and Solution Using Gothert's Rule, M17 Bomb Shape, $\alpha = 0^\circ$, $M_\infty = 0.8$

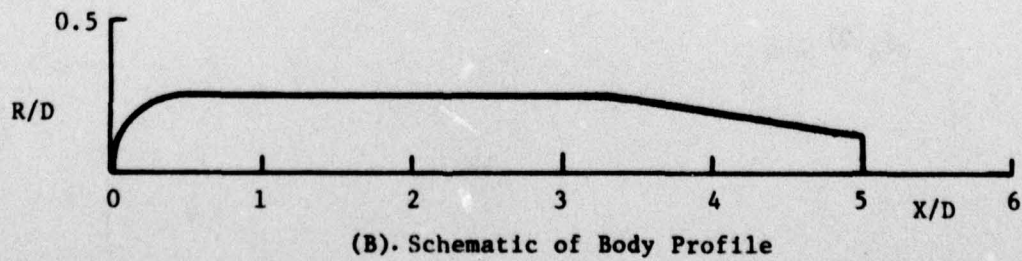
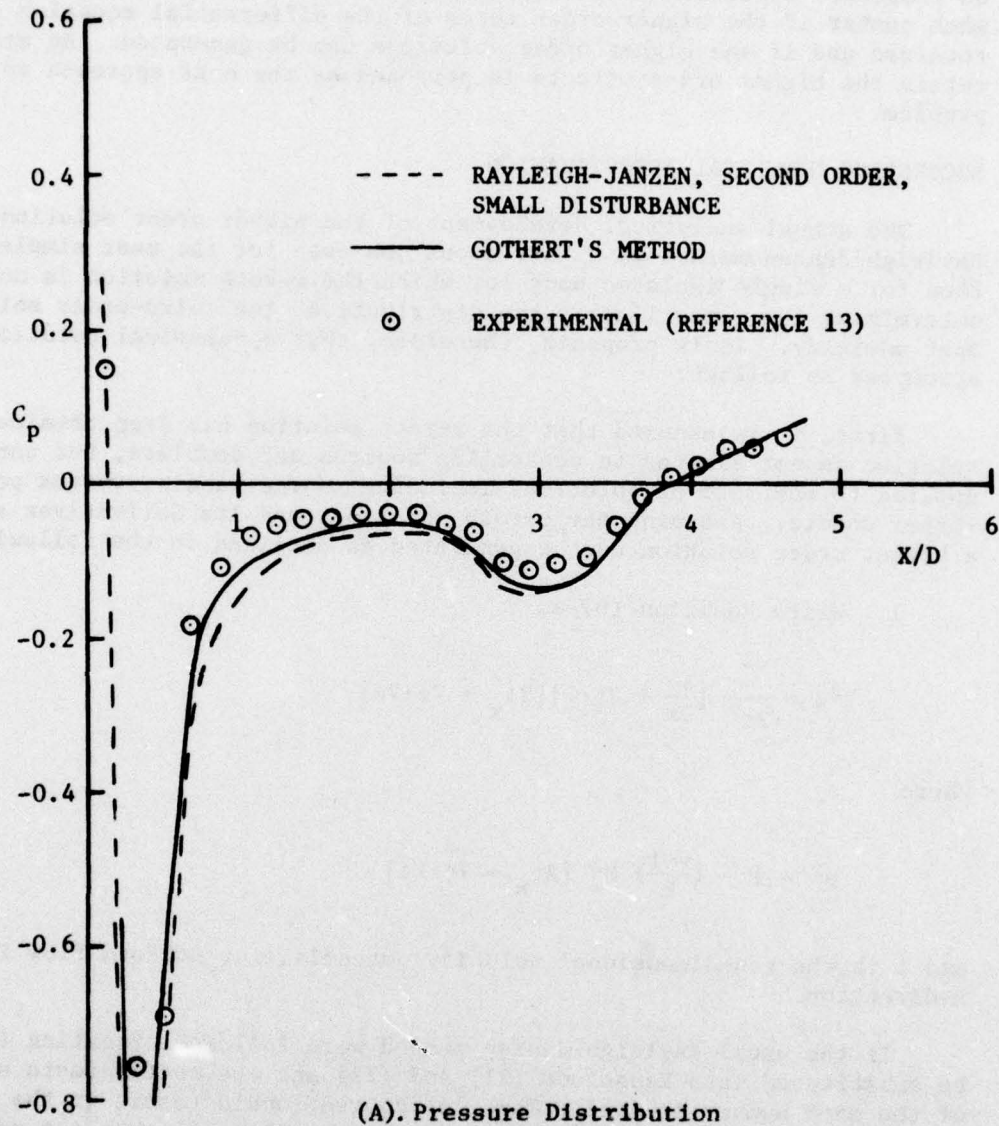


Figure 4. Comparison of Rayleigh-Janzen Solution and Solution Using Gothert's Rule with Maximum Volume Bombs Shape, $\alpha = 0^\circ$, $M_\infty = 0.5$

It seems evident, therefore, that the Rayleigh-Janzen solution technique, at least through the second-order solution, will not be significantly better at predicting the aerodynamic loads near and at the critical mach number than the much simpler technique using Gothert's Rule. It still may be possible, however, to use the Rayleigh-Janzen solution at the critical mach number if the higher order terms of the differential equation can be retained and if the higher order solutions can be generated. An attempt to retain the higher order effects is proposed as the next approach to the problem.

SUCCESSIVE NUMERICAL APPROXIMATION

The actual analytical development of the higher order solutions by the Rayleigh-Janzen method is a horrendous job even for the most simple case. Even for a single isolated body for which the zeroth solution is obtained by determining the centerline source distribution, the third-order solution is most unwieldy. It is proposed, therefore, that a numerical solution be attempted as follows:

First, it is assumed that the zeroth solution has been obtained. This solution is not limited to centerline sources and doublets, but can be applied to any form of solution, including source panels, vortex panels, and vortex sheets. Assuming the zeroth solutions and its derivatives are known, a higher order solution can be generated as outlined in the following steps.

1. Write Equation (6) as

$$\nabla^2 \phi = \frac{M_\infty^2}{2a^2} \left[\frac{\partial}{\partial x} + \nabla \phi \cdot \nabla \right] [2\phi_x + \nabla \phi \cdot \nabla \phi] \quad (21)$$

where

$$a^2 = 1 - \left(\frac{\gamma-1}{2} \right) M_\infty^2 [2\phi_x + \nabla \phi \cdot \nabla \phi] \quad (22)$$

and ϕ is the non-dimensional velocity potential for uniform flow in the x-direction.

If the usual Rayleigh-Janzen method were followed, Equation (7) would be substituted into Equations (21) and (22) and the coefficients of powers of the mach number equated. This, of course, would result in the ordered solutions as previously considered. It is easily seen that the zeroth solution would be the solution obtained by solving the Laplace equation written as

$$\nabla^2 \phi^{(0)} = 0 \quad (23)$$

The solution of this equation will also be taken as the first step in this method. However, the actual method of solving Equation (23) is unimportant to this approach.

2. The next (and all successive) steps will follow the usual successive approximation method. Thus, to the next approximation, Equation (21) can be written as

$$\nabla^2 \phi^{(1)} = F(\phi^{(0)}) \quad (24)$$

where the complete boundary condition is to be applied to the solution for $\phi^{(1)}$, and $F(\phi^{(0)})$ is the right-hand side of Equation (21) expressed in terms of $\phi^{(0)}$.

3. Write the first approximation as the sum of the particular and complimentary solutions which can be expressed as

$$\phi^{(1)} = \phi_c^{(1)} + \phi_p^{(1)} \quad (25)$$

where the particular solution must satisfy the partial differential equation

$$\nabla^2 \phi_p^{(1)} = F(\phi^{(0)}) \quad (26)$$

while the complimentary solution must satisfy the equation

$$\nabla^2 \phi_c^{(1)} = 0 \quad (27)$$

and Equation (25) must satisfy the boundary conditions.

The particular solution can be determined throughout the flow field by numerical techniques. However, if the only points of interest for a single body are those lying on the body surface, the size of the numerical grid can be greatly reduced. If two or more bodies with mutually interfering flow fields are considered, a grid system which envelops all bodies must be used. This system could still be two or more orders of magnitude smaller than that required by other numerical techniques.

4. Successive approximations can be generated by replacing the zeroth solution, $\phi^{(0)}$, with the first approximation $\phi^{(1)}$, and repeating steps 2 and 3.

The classical Rayleigh-Janzen method is valid only for subcritical mach numbers. Conceptually, however, this approach could be made useful for transonic and perhaps supersonic flows by taking into account von Kármán's Rule for Forbidden Signals.

An alternate formulation for this method which might greatly speed up convergence for the subsonic case and help to implement the supersonic solution is as follows:

1. Write Equation (21) as

$$\nabla^2 \phi - M_\infty^2 \phi_{xx} = M_\infty^2 \left\{ \frac{1}{2a} \left[\frac{\partial}{\partial x} + \nabla \phi \cdot \nabla \right] [2\phi_x + \phi_x^2 + \phi_y^2 + \phi_z^2] - \phi_{xx} \right\} \quad (28)$$

2. For the subsonic case, this results in the zeroth solution which is the solution to the Prandtl-Glauert equation

$$(1-M_\infty^2) \phi_{xx} + \phi_{yy} + \phi_{zz} = 0 \quad (29)$$

The solution of this equation using Gothert's Rule is compared with the Rayleigh-Janzen method in Figures 3 and 4.

3. For the supersonic case the zeroth solution is the solution of the classical wave equation written as

$$(M_\infty^2 - 1) \phi_{xx} - \phi_{yy} - \phi_{zz} = 0 \quad (30)$$

Several techniques are known for solving this equation.

Further evaluation of the use of Equations (28), (29), and (30) will be required before their use in this successive approximation scheme can be validated.

SECTION III

EXACT NUMERICAL SOLUTION, PURVIS METHOD

INTRODUCTION

The analytical approaches found in References 1 through 10 and the methods discussed in the previous section do not seem to be adequate at speeds approaching the critical mach number which is the speed range of most interest for this study. This inadequacy seems to be due to the fact that the previous methods have used linearized potential flow theory, and at speeds approaching critical mach number, the neglected nonlinear terms become dominant.

In this study, an attempt is made to provide an analytical foundation for a method which may ultimately be used to solve the full nonlinear potential flow field about any configuration. The problem is doubly complicated due to the nonlinear partial differential equation (PDE) involved and the fact that the domain is fully elliptic; i.e., disturbances at any point are felt everywhere in the flow field. Since the problem is nonlinear, it is felt that a numerical scheme must be used.

The major numerical methods for solving a nonlinear PDE of this type are Finite Difference (Relaxation and Time Dependent asymptotic approach to steady state), Finite Elements, Method of Integral Relations, and Method of Projections.

Comprehensive surveys and descriptions of these techniques and applications may be found in references such as References 14 and 15 and will not be discussed here. Most of these methods have been eliminated from consideration due to excessive computer run times or storage requirements and complexity of the coding.

The current work presents a much simpler numerical method for solving the full nonlinear potential equation than those found in the literature. The ensuing analysis uses some of the more desirable concepts of several of the above techniques to minimize solution time and complexity and simplify the treatment of body boundary conditions

In general, the approach blends the finite element and finite difference concepts into a method for solving the full potential equations in a conservation form. The problem formulation leads to a large system of equations which is solved iteratively. The solution does not require storing or inverting a large coefficient matrix and proceeds in such a manner that disturbances can propagate and be felt at all points in the field during the solution.

GOVERNING EQUATION

Under the assumptions of steady, adiabatic, inviscid flow, the equations for conservation of mass, momentum, and energy and the ideal gas equation of state may be combined into a single differential equation. A further restriction of irrotationality allows the introduction of the velocity potential. The governing equation may then be expressed as

$$\nabla \cdot (\rho \nabla \phi) = 0 \quad (31)$$

where ϕ is the nondimensionalized total velocity potential. Since the flow is isentropic, the non-dimensional density ρ may be expressed in terms of the velocity potential as

$$\rho = \left[1 + \frac{\gamma-1}{2} M_\infty^2 (1 - \nabla \phi \cdot \nabla \phi) \right]^{\frac{1}{\gamma-1}} \quad (32)$$

Equation (31), when expanded using the components of the del operator ∇ and put in terms of the non-dimensional perturbation potential, is the familiar full potential equation.

DIVERGENCE INTEGRAL

To formulate the problem for a computer solution, the divergence theorem is applied to the integral form of the governing Equation (31). Integrating over an arbitrary volume V yields

$$\int_V \nabla \cdot (\rho \nabla \phi) dV = \oint_S \rho \nabla \phi \cdot \hat{n} dS = 0 \quad (33)$$

where S is the boundary surface enclosing V and \hat{n} is the unit outward normal on S .

The surface integral form of Equation (33) is solved numerically as discussed in the following subsections.

GENERAL SOLUTION

As in other numerical methods, the domain in which Equation (33) is to be solved is subdivided with a rectangular mesh or grid, and initial values of ρ are assumed at the center of each cell in the grid. The surface integral form of Equation (33) is applied to each cell in the grid and is written in terms of the potential at the center of each cell. The resulting system of equations is solved by successive over-relaxation and subject to the usual boundary conditions of no flow normal to body surfaces and uniform flow at infinity. The values of ϕ thus found are then differenced, and new

values for ρ in each cell are obtained using Equation (32). This process is repeated until values of ρ in each cell have converged to within a desired percentage for several successive cycles.

CELL FORMULATION

For two-dimensional and axisymmetric flows, the surface integral form of Equation (33) as applied to cell (i,j), shown in Figure 5, is:

$$\rho_1 u_1 S_1 + \rho_2 v_2 S_2 - \rho_3 u_3 S_3 - \rho_4 v_4 S_4 = 0 \quad (34)$$

To obtain Equation (34), the sign on Equation (33) was changed and the integral was evaluated assuming a linear distribution of ρu or ρv along each surface S.* The values in Equation (34) are then the values at the center of each surface, or, equivalently, the average of ρu or ρv along S.

Expressed in terms of values at the center of the cell, the terms in Equation (34) are

$$\rho_1 = \frac{1}{2} (\rho_{i,j} + \rho_{i-1,j}) \quad (35)$$

and

$$u_1 = \frac{\phi_{i,j} - \phi_{i-1,j}}{\Delta x} \quad (36)$$

Equation (36) is the standard centered difference formula and is accurate to order $(\Delta x)^2$. The areas in Equation (34) differ for 2-D and axisymmetric flow. Referring to Figure 5, the areas for 2-D flow are

$$S_1 = y_{e_{j+1}} - y_{e_j} \quad (37)$$

$$S_2 = x_{e_{i+1}} - x_{e_i} \quad (38)$$

where a unit depth has been assumed. For the 3-D axisymmetric case, the areas are

$$S_1 = \pi y_{e_{j+1}}^2 - \pi y_{e_j}^2 \quad (39)$$

$$S_2 = (2\pi y_{r_j})(x_{e_{i+1}} - x_{e_i}) \quad (40)$$

*Equivalent to assuming a second-order distribution of ϕ along each cell surface in the Finite Element method.

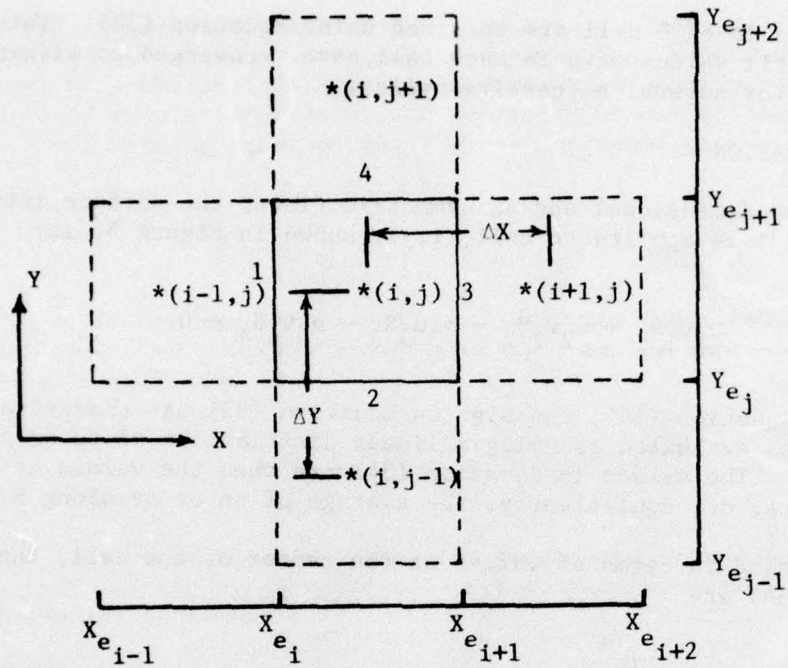


Figure 5. Schematic of Computational Cell

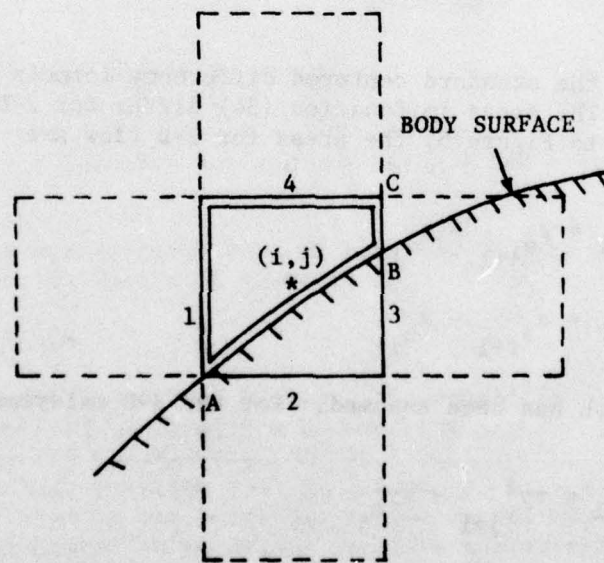


Figure 6. Schematic of Body Boundary Cell

Using the appropriate forms of Equations (35) through (40), Equation (34) can be rearranged into

$$A1\phi_{i-1,j} + A2\phi_{i,j-1} + A3\phi_{i+1,j} + A4\phi_{i,j+1} + A5\phi_{i,j} = 0 \quad (41)$$

where, for example,

$$A1 = - (\rho_{i,j} + \rho_{i-1,j}) S_1 / 2\Delta x \quad (42)$$

and

$$A5 = - (A1 + A2 + A3 + A4) \quad (43)$$

In matrix formulation, this is a banded, diagonally dominant matrix, and thus an iterative method such as accelerated Gauss-Seidel (successive over-relaxation) will always converge. Note that Equation (34) is exact in the limit of vanishing cell size and that only 1st derivatives of the dependent variable are required. The finite difference equations used for u and v are accurate to order $(\Delta x)^2$ and $(\Delta y)^2$, respectively.

BODY BOUNDARY CONDITIONS

One of the most difficult aspects of finite difference methods to date has been the treatment of body conditions, while the opposite is true in the finite-element method since the body surface forms the sides of some elements. The present formulation combines the simplicity of calculations of the finite-difference method with the relatively simple but exact finite-element treatment of body boundary conditions. Consider the cell cut by the body surface as shown in Figure 6. The surface integral for this cell is around the boundary shown by the double solid line. Since the body boundary condition of no flow normal to the surface ($\vec{V} \cdot \hat{n} = 0$) requires that there be no flow through surface AB, then the equivalent expression of Equation (34) is

$$\rho_1 u_1 S_1 - \rho_3 u_3 S_3 - \rho_4 v_4 S_4 = 0 \quad (44)$$

where S_3 is now the area of segment BC. Note that this equation is exact for any size cell, and that no interpolation, contour mapping, or other scheme is required as with general finite-difference methods.

STRETCHED COORDINATES

Since it is desirable to keep the number of cells at a minimum, for some problems it is necessary to employ nonlinear cell stretching to place the

outer boundaries at infinity. A stretched coordinate capability is provided using

$$x = \tan \xi \quad (45)$$

$$y = \tan \theta \quad (46)$$

From the chain rule, the finite-difference derivatives become, for example:

$$u_1 = \phi_x \Big|_1 = \frac{\partial \phi}{\partial \xi} \frac{\partial \xi}{\partial x} \Big|_1 = \frac{\phi_{i,j} - \phi_{i-1,j}}{\Delta \xi} \frac{1}{1 + x_e^2} \quad (47)$$

Hence, a uniform rectangular grid in ξ, θ can be used, and the difference equations are accurate to order $(\Delta \xi)^2, (\Delta \theta)^2$, respectively. The areas of the cell sides are the same as before, e.g.,

$$S_2 = s_{e_{i+1}} - x_{e_i} \quad (48)$$

INITIAL CONDITIONS

With any numerical method, the closer the initial guess is to the answer, the faster the convergence. In the present scheme a simplified form of Slender Body Theory, using superimposed solutions from the linearized potential equation, is employed to generate initial values of ϕ and ρ in the grid. Each centerline segment of the body lying in a cell is assumed to be a constant strength source filament. The strength is proportional to the value of the body surface alone as evaluated at the midpoint of the segment. The initial value of ϕ at any point is then the sum of the contributions from each segment.

COMPARISON WITH EXPERIMENTAL DATA

Figures 7 through 10 present comparisons of theory with experiment for several two-dimensional and three-dimensional axisymmetric bodies. The figures have experimental and theoretical values of pressure coefficient C_p plotted versus non-dimensional body lengths.

Figure 7 presents data for a 6-percent-thick parabolic arc airfoil in two-dimensional flow. Figure 7(A) has a free stream mach number of 0.707, and Figure 7(B) has M_∞ equal to 0.817. The body is twenty cells long and one cell high. In both cases the flow is subcritical, and the critical pressure coefficient C_p^* is listed on the figure and shown on the axis where

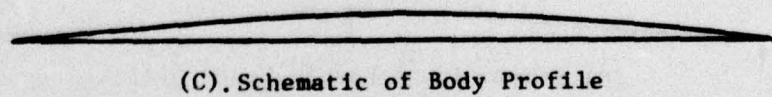
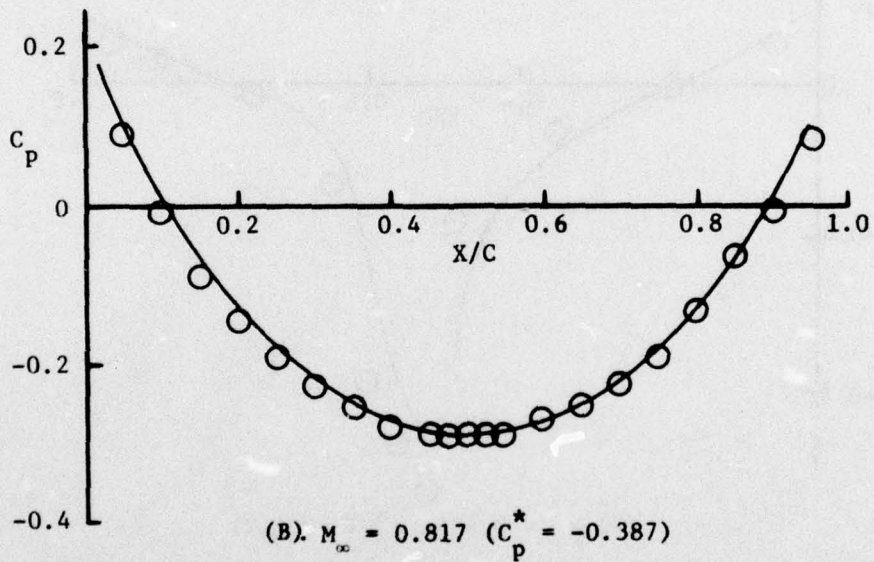
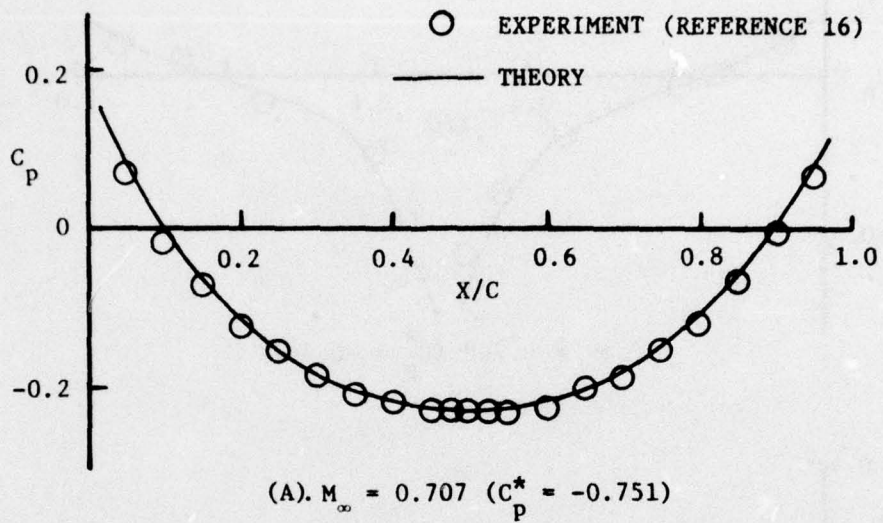
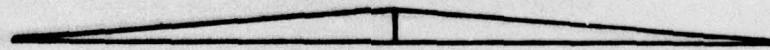
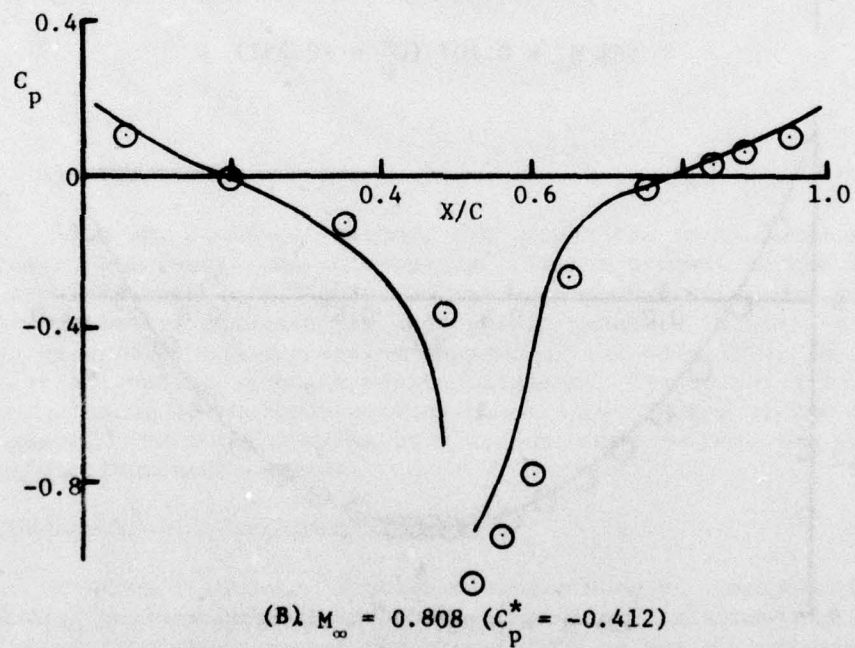
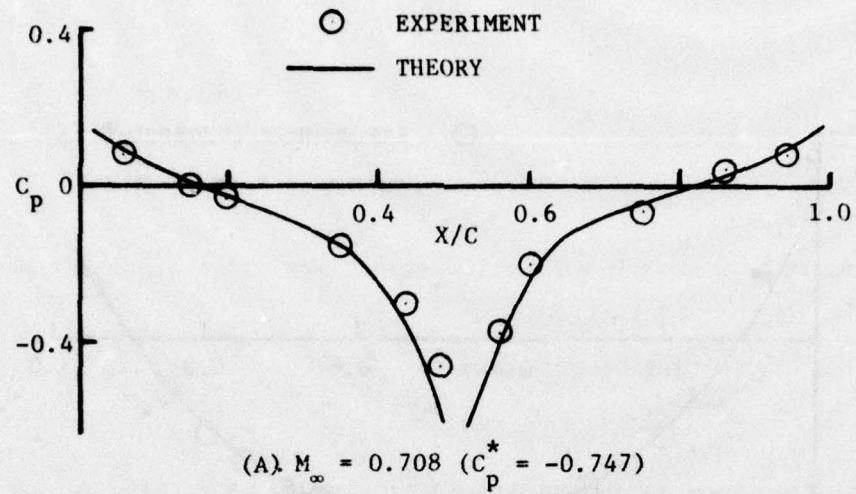


Figure 7. Comparison of Numerical Solution Using Purvis Method and Experiment for a 6-Percent Parabolic Arc Airfoil



(C) Schematic of Double Wedge Airfoil

Figure 8. Comparison of Numerical Solution Using Purvis Method and Experiment for Double Wedge Airfoil

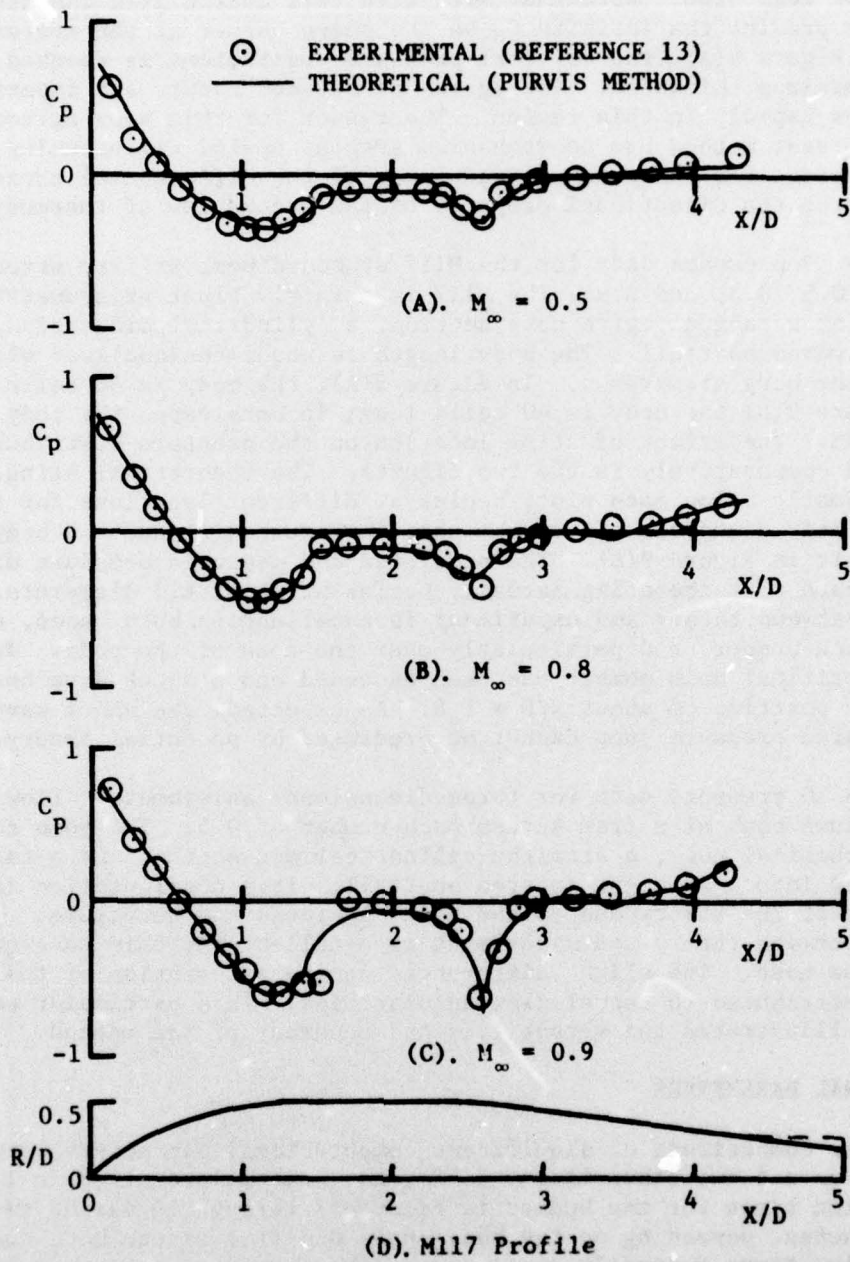


Figure 9. Comparison of Numerical Solution Using Purvis Method and Experiment for M117 Bomb Shape

appropriate. The flow is close to reaching critical in Figure 7(B). The agreement between theory and experiment is excellent in both cases.

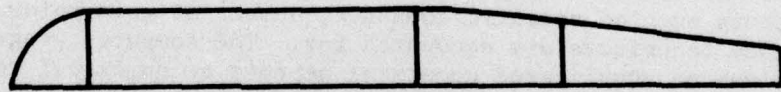
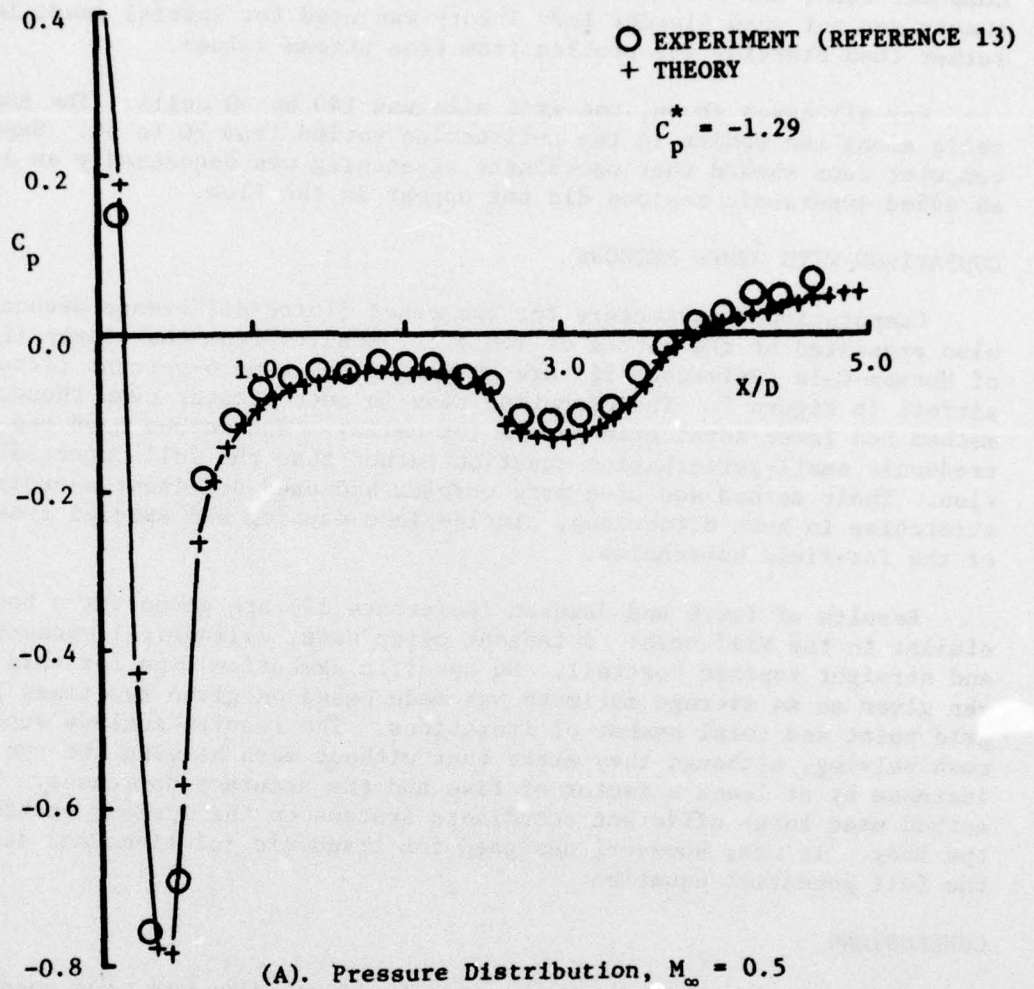
Figure 8 presents the same type of data for two-dimensional flow over a double wedge with a half-angle of 4.5 degrees. The body is twenty cells long and one cell high. Note that even with this coarse grid the theory attempts to predict the infinite C_p on the sharp corner at the center of the wedge. In Figure 8(A), the critical pressure coefficient is reached near the wedge maximum thickness. The agreement between theory and experiment deteriorates rapidly in this region. The reason for this poor agreement is that the current method has no mechanism such as upwind differencing to properly account for the zone of dependence of the differential equations and to enforce the directional property of the second law of thermodynamics.

Figure 9 presents data for the M117 standard bomb at free stream mach numbers of 0.5, 0.8, and 0.9. The M117 is a fairly blunt axisymmetric body consisting of a tangent ogive nose section, a cylindrical midsection, and a straight-tapered boattail. The body length is nondimensionalized with respect to the body diameter d . In Figure 9(A), the body is 48 cells long and in Figure 9(B) the body is 40 cells long; in both cases the body is 5 cells high. The effect of sting location on the pressure distribution is illustrated comparatively in the two figures. The theoretical sting, shown in the schematic below each plot, begins at different locations for the two cases, 4.8 body diameters aft of the nose in Figure 9(A) and 4.0 body diameters aft in Figure 9(B). The predicted and measured pressure distributions indicate that the sting actually begins at about 4.3 diameters. The agreement between theory and experiment is excellent in both cases, even at the high Mach number, and particularly over the nose of the body. In Figure 9(C), the critical mach number has been exceeded and a shock wave has formed at an axial position of about $x/D = 1.6$. As expected, the shock wave and its associated pressure jump cannot be predicted by potential theory.

Figure 10 presents data for three-dimensional axisymmetric flow over a maximum volume bomb at a free stream mach number of 0.5. The bomb consists of a hemispherical nose, a straight cylindrical midsection, and a tangent ogive faired into a straight tapered boattail. This configuration is a severe test of the theory due to the nose bluntness and curvature. Overall agreement between theory and experiment is excellent for this case particularly on the nose. The slight differences on the aft section of the body have been attributed to tunnel flow angularities. This particular configuration best illustrates the versatility and accuracy of the method.

COMPUTATIONAL PARAMETERS

Further comparisons of significant computational parameters between the various cases and two other finite-difference methods are given in Table 1. The execution times for the bodies in Figures 7 through 10 varied from 3 to 10 minutes, depending on the body shape and free stream mach number. The execution times generally increased as the free stream Mach number was increased. The longest run time was for the maximum volume bomb; this was



(B). Body Profile

Figure 10. Comparison of Numerical Solution Using Purvis Method and Experiment for 16-Inch Maximum Volume Hemispherical Nose Bomb

attributed to the large velocity gradients in the nose region. In separate computer runs, the execution times for the M117 bomb decreased from ten to twenty percent when Slender Body Theory was used for initial conditions rather than starting the problem from free stream values.

For all cases shown, the grid size was 140 by 50 cells. The number of cells along the bodies in the x-direction varied from 20 to 68. Separate computer runs showed that coordinate stretching was unnecessary as long as embedded supersonic regions did not appear in the flow.

COMPARISON WITH OTHER METHODS

Computational parameters for two other finite-difference methods are also presented at the bottom of Table 1. Results from the pioneering work of Murman-Cole (Reference 16) are shown for the same 6-percent circular arc airfoil in Figure 7. The execution time is much greater even though their method had fewer total grid points (or cells). The method used the transonic small-perturbation equation rather than the full potential equation. Their method was also more complex and used nonlinear coordinate stretching in both directions, circle-plane mapping and special treatment of the far-field boundaries.

Results of South and Jameson (Reference 17) are given for a body similar to the M117 bomb: a tangent ogive nose, cylindrical midsection, and straight tapered boattail. No specific execution time for this case was given so an average estimate was made based on given run times per grid point and total number of iterations. The results include successive mesh halving, although they state that without mesh halving the run times increase by at least a factor of five and the accuracy decreases. The method used three different coordinate systems on the various sections of the body. It was, however, designed for transonic solutions and did solve the full potential equation.

CONCLUSIONS

The present method is computationally fast, accurate, and compares well with experiment. Computation times are better than other methods when all factors such as specific computer, number of grid points, and special convergence techniques are accounted for. The computer program is simple and involves no complicated numerical schemes or empirical techniques. For all cases considered, coordinate stretching was found to be unnecessary, although the method is restricted to flows with no embedded supersonic regions. No problems were encountered for blunt body cases or near $r=0$ for axisymmetric flows, and no special treatment was necessary for these regions or for handling the boundary conditions on body surfaces.

RECOMMENDATIONS

The present method has proven to be sufficiently fast, simple, and accurate. For solving large problems such as two- and three-body interference flows, the following modifications are recommended:

TABLE 1. COMPARISON OF COMPUTATIONAL PARAMETERS

CONFIGURATION	M	BODY CELLS	TOTAL CELLS	COORDINATE STRETCHING	INITIAL CONDITIONS	EXECUTION TIME	COMPUTER
		X	Y				
6 PERCENT CIRCULAR ARC AIRFOIL	0.707	20	140	50	SBT*	2m50s	IBM 370/150 (ALL)
	0.817	20	140	50	SBT	3m22s	
9 DEGREE DOUBLE WEDGE	0.708	20	140	50	SBT	2m58s	
	0.808	20	140	50	SBT	5m17s	
M117 STANDARD BOMB	0.5	48	140	50	ρ_{∞} V_{∞}	4m21s	
	0.8	40	140	50	ρ_{∞} V_{∞}	4m45s	
	0.9	40	140	50	ρ_{∞} V_{∞}	12m11s	
16-INCH MAXIMUM VOLUME BOMB (REF. 13)	0.5	68	140	50	SBT	9m54s	
MURMAN & COLE (REF. 8)	0.817	40	74	41	UNKNOWN	30m	IBM 360/44
6 PERCENT CIRCULAR ARC					x AND y		
SOUTH AND JAMESON (REF. 9)	0.83	UNKNOWN	193	49	SPECIAL COORDINATES	3m30s**	CDC 6600
BODY SIMILAR TO M117							

*SBT-Slender Body Theory

**An Average Time with Mesh Halving

- (1) Use of line relaxation to reduce storage and perhaps accelerate solution convergence.
- (2) Incorporate a successive mesh refinement scheme, such as that of Reference 17 which could reduce execution time by a factor of five.
- (3) Use a linearized planar wing-pylon solution for wing-store interference.
- (4) Use previous methods such as Reference 6 for initial conditions and far-field boundary conditions.
- (5) Add upwind differencing or some equivalent scheme to allow extension of the method above critical mach numbers.

SECTION IV

DISCUSSION OF BOUNDARY LAYER STUDY

INTRODUCTION

As can be seen by reading the literature, no one to date has solved the three-dimensional turbulent boundary layer shock interaction problem. The basic reason stems from two distinct areas: (1) the mathematical modeling of the flow field and (2) the viscosity model for turbulent flow. In spite of these problems, however, attempts to model the flow in the present work were carried out using a simple eddy viscosity formulation. Most of the work was done in generating an external flow field and coupling the inviscid field to the viscous boundary layer. Because of computation time and storage on the computer, techniques were used which would require minimal time and storage. For this reason, solutions of the Navier Stokes equations were eliminated from consideration at the outset. It was also decided that (1) the general interference potential flow solution already developed in past research efforts would be utilized to generate the basic inviscid solution; (2) three-dimensionality must be considered; and (3) compressible turbulent flow must be incorporated into the solution. Because of these restrictions, the boundary layer equations approach was used in the formulation of the viscous flow region. In this region, the basic equations were taken from the work of Sasman and Cresci (Reference 18).

MATHEMATICAL APPROACH

The idea in the present work was to develop a technique which would couple the present three-dimensional potential flow solution of the three stores mounted on a triple ejector rack to a two-dimensional boundary layer formulation. This concept is feasible if discrete streamlines located at the edge of the boundary layer could be identified as shown in Figure 11. Since the boundary layer is generally thin, the layer of fluid immediately below the streamline, i.e., between the streamline and the actual body surface, can be considered to be two-dimensional in nature in which the two-dimensional boundary layer equations apply. That is, even though the streamline may curve around the body and the plane defined by the streamline and the shadow of the streamline on the body is a curved surface, the thickness is much less than the body characteristic dimension and thus may be approximated by two-dimensional boundary layer equations. Hence, a clear accurate definition of a streamline near the body surface is essential to the problem solution.

The mechanics of generating this streamline is rather simple. First, the potential flow solution is generated for the system of bodies chosen to be analyzed. Then a point in space (x_0, y_0, z_0) is chosen near the body surface and near the nose of the body. At this point, using the potential

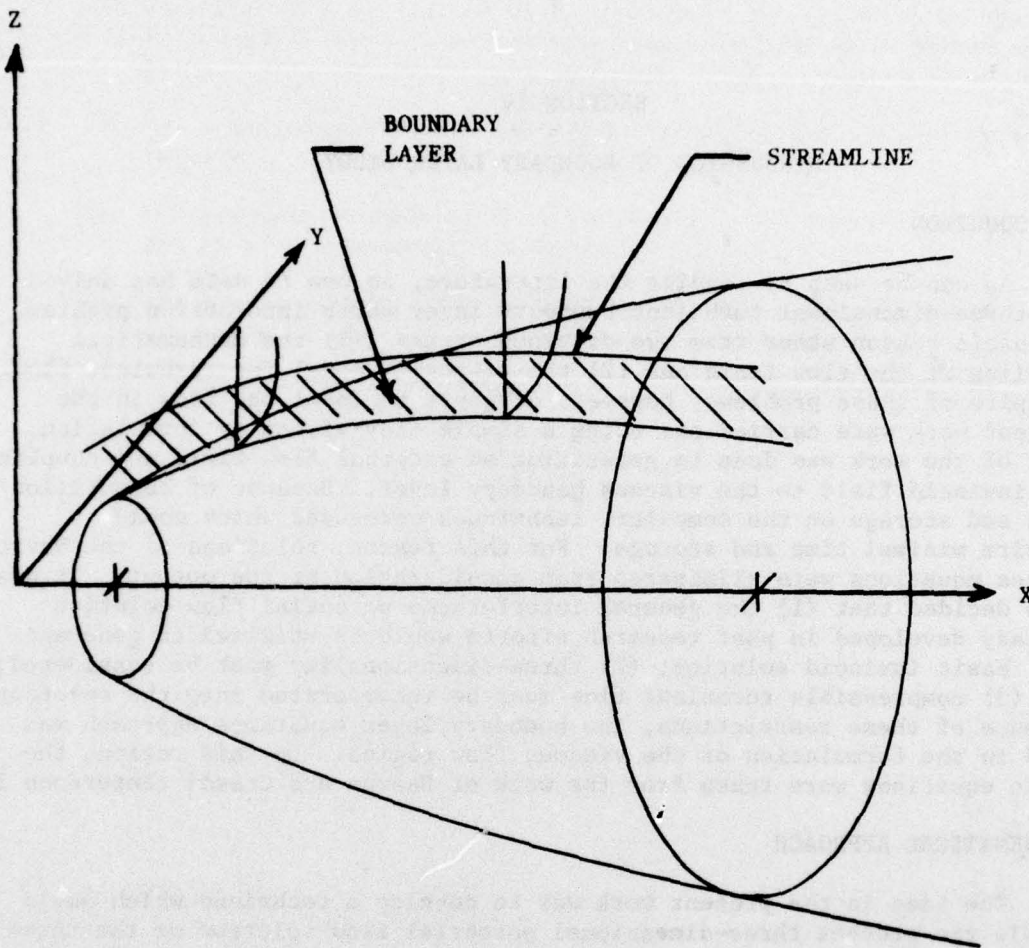


Figure 11. Axisymmetric Body with a Curved Boundary Layer Plane

solution already determined, the velocity components u' , v' , and w' are determined. Adding the free stream components appropriately, we then have

$$u = V_{\infty} \cos \alpha + u' \quad (49)$$

$$v = V_{\infty} \sin \alpha + v' \quad (50)$$

$$w = w' \quad (51)$$

where α is the body angle of attack. Then it is assumed that over a very small but finite time interval the new positional coordinates of the streamline may be approximated by

$$x_{\text{new}} = x_0 + u\Delta t, \quad (52)$$

$$y_{\text{new}} = y_0 + v\Delta t,$$

and

$$z_{\text{new}} = z_0 + w\Delta t.$$

Computation of the new fluid velocity at the new location is then carried out, and the process is repeated. In this manner a matrix of streamline coordinate locations is defined. This method suffers from one major drawback. Any error induced in the coordinate location at any upstream point is carried to the next location and accumulates. However, large error buildup can be avoided by the use of small time intervals, Δt . The coordinates of these points on the streamline are also used to determine the step interval for the boundary layer computations, and the velocity at the edge of the boundary layer is always known as well as the external free stream pressure.

This section of the program and analysis proved to be rather successful in that discrete streamlines beginning anywhere near the body surface were identified. Problems were encountered near the aft end of the body where the streamline deviated from the body and trailed off in the free-stream direction. This problem was attributed to the characteristic nature of point source solutions for the potential flow field in which the induced velocity component u tends to oscillate.

Boundary layer computations using this scheme were carried out with some degree of success. However, the interaction problem using this approach has not been solved.

CONCLUSIONS

After several computer runs, more literature studies, and much thought, it is believed that the approach taken here will not yield the desired results. This conclusion is based on the following observations:

1. The shock boundary layer interaction is strongly dependent on its three-dimensional geometry.
2. In the boundary layer equations approach, the boundary layer only reacts to its external flow field; hence this field must be very accurate if accurate results are obtained. Provisions using this scheme must be made for transmission of disturbances upstream in the boundary layer or in regions where $M < 1.0$ (elliptic equations in the potential field) and must obey the hyperbolic equations for regions where $M > 1.0$.
3. At present, the Navier Stokes solution approach requires too much computer time and storage.
4. Turbulent mixing models are inadequate to model the shear stresses in the interaction region.
5. It appears that much more work in viscous aerodynamics will be required before adequate results will be obtained by pure analytical methods.

SECTION V

DISCUSSION OF FINITE ELEMENTS STUDY

INTRODUCTION

The analysis of subsonic flow requires the solution of partial differential equations of the elliptic type. The solution of these equations can be obtained by the traditional Finite Difference Methods, as mentioned in Section III. One of the inherent difficulties with the Finite Difference Method, which is not significant in the finite element method, is that special differencing techniques must be incorporated to handle irregular or curved boundaries. Since the difference formulas used for these boundaries are usually of lower-order accuracy than the formulas used for the rest of the flow field and since in subsonic flow disturbances at any point in the flow region are felt throughout the flow region, the overall accuracy of the solution is reduced. This inexact treatment of the boundaries is a limitation to the Finite Difference Method although very accurate solutions may be obtained by using a large number of grid points or by using higher order difference formulas. However, the incorporation of more accurate formulas in the Finite Difference Method usually complicates the treatment of the boundaries.

In the last decade much effort has been directed toward the application of the Finite Element Method to fluid flow problems. Although it was originally developed in the aircraft industry for solution of complex structural problems, the Finite Element Method is readily applicable to all types of boundary value problems (see Reference 19). An application of this method to incompressible inviscid potential flows is given by Martin (Reference 19). Zienkiewicz (Reference 15) gives an application to incompressible viscous flow problems. Huebner (Reference 20) devotes an entire chapter to various methods which have been successfully used to solve both viscous incompressible and inviscid compressible flows. Reference 21 presents numerous analyses of fluid flow problems which have been solved by the Finite Element Method.

A particular formulation given by Heubner (Reference 20) has been used by a number of researchers to obtain solutions to inviscid compressible flows. This formulation, in a slightly modified form, has been chosen in this study to obtain solutions to two-dimensional flow over a circular arc airfoil for mach numbers where compressibility effects are significant. The governing equation and the basic iteration are the same as those used in Section III of this report. The formulation and numerical technique, however, are significantly different.

GOVERNING EQUATIONS

The governing equations in this study are the same as used in Section III. Repeated here for continuity, the conservation equations for steady, adiabatic, inviscid flow of an ideal gas may be combined to give the equations

$$\nabla \cdot (\rho \nabla \phi) = 0 \quad (55)$$

and

$$\rho = \left[1 + \left(\frac{\gamma-1}{2} \right) M_\infty^2 (1 - \nabla \phi \cdot \nabla \phi) \right]^{\frac{1}{\gamma-1}} \quad (56)$$

where ϕ is the nondimensional velocity potential, and ρ is the nondimensional density.

SOLUTION PROCEDURE

Equations (55) and (56) are the basis of a rapidly convergent iterative method for solution of compressible flow problems. The first step involves assuming $\rho = 1$ throughout the flow field as an initial estimate. Then Equation (55) is used to derive a system of linear algebraic equations which may be solved for values of velocity potential ϕ . The resulting values of ϕ are then numerically differentiated to obtain values of the velocity components which are used in Equation (56) to compute new values of density which, in turn, are used in Equation (56) and the process is repeated. The iteration is continued until the densities no longer change from one iteration to the next. The pressures are then computed using Equation (57).

$$C_p = \frac{2}{\gamma M_\infty^2} \left\{ \left[1 + \frac{\gamma-1}{2} M_\infty^2 (1 - \nabla \phi \cdot \nabla \phi) \right]^{\frac{\gamma}{\gamma-1}} - 1 \right\} \quad (57)$$

which is the usual expression for pressure coefficient for compressible flow.

FINITE ELEMENT FORMULATION

The flow field in which the solution is obtained is an infinite domain surrounding a two-dimensional 6-percent circular arc airfoil. The far-field domain is approximated by placing the computational boundaries three body lengths away from the body in all directions and forms a rectangular region enclosing the body. The far-field boundary condition used is that of uniform flow in the x direction and expressed in terms of the velocity potential is given by Equation (58)

$$\phi = V_\infty x \quad (58)$$

The body boundary condition is the usual flow tangency condition expressed by Equation (59)

$$\rho \nabla \phi \cdot \hat{n} = 0 \quad (59)$$

where \hat{n} is a unit vector normal to the body surface.

For computational purposes, these mixed boundary conditions are formulated as given by Equations (60) and (61).

$$\rho \nabla \phi \cdot \hat{n} = f(x, y, z) \text{ on } S_2 \quad (60)$$

and

$$\phi = g(x, y, z) \text{ on } S_1 \quad (61)$$

where S_1 and S_2 are portions of the boundary and f and g are prescribed functions of position (see Figure 12).

The finite element solution technique is based on a variational principle derived from the calculus of variations which, when expressed in terms of the velocity potential, minimizes the functional

$$I(\phi) = \frac{1}{2} \int_{\Omega} \rho \nabla \phi \cdot \nabla \phi \, d\Omega - \int_{S_2} \phi f \, dS_2 \quad (62)$$

and satisfies Equations (55), (56), and (61).

To apply this method, the rectangular region is subdivided into triangles and the values of ϕ are interpolated over the area of the triangle by means of a set of Lagrangian interpolation functions. These interpolation formulas are most conveniently represented in terms of the natural coordinates (sometimes called area coordinates) defined by the equations

$$x = L_1 x_1 + L_2 x_2 + L_3 x_3 \quad (63a)$$

$$y = L_1 y_1 + L_2 y_2 + L_3 y_3 \quad (63b)$$

$$1 = L_1 + L_2 + L_3 \quad (63c)$$

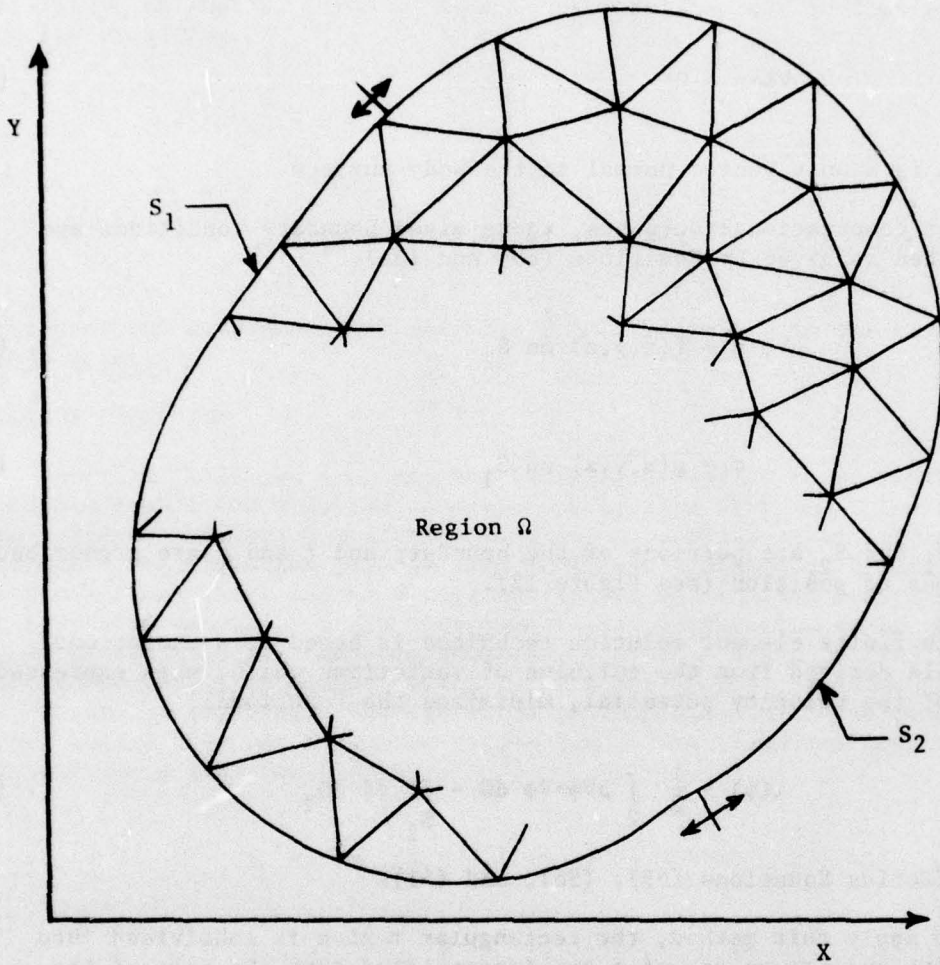


Figure 12. Schematic of Body Boundary Condition Coordinates for Finite Element Analysis

where (x_1, y_1) , (x_2, y_2) , (x_3, y_3) are the vertices of the triangle in plain rectangular coordinates. Solving Equations (63a, b, c) for L_1 , L_2 , and L_3 yields the general form

$$L_i = a_i + b_i x + c_i y, \quad i = 1, 2, 3 \quad (64)$$

where a_i , b_i , and c_i are constants.

For linear interpolation between vertices of the triangle, the interpolation functions are given by

$$N_i = L_i \quad (65)$$

For second-order interpolation they are given by

$$\begin{aligned} N_1 &= L_1^2 - L_1(L_2 + L_3) \\ N_2 &= L_2^2 - L_2(L_3 + L_1) \\ N_3 &= L_3^2 - L_3(L_1 + L_2) \\ N_4 &= 4L_1L_2 \\ N_5 &= 4L_2L_3 \\ N_6 &= 4L_3L_1 \end{aligned} \quad (66)$$

where the node numbers 1 to 6 are shown in Figure 13.

The nodal values of ϕ are used to define the variation of ϕ over a triangular element by the following expression

$$\phi^{(e)} = \sum_1 N_i \phi_i \quad (67)$$

After the interpolation functions are chosen, they are substituted into Equation (62) and then the minimization process is carried out on an element-by-element basis. This is done by requiring that

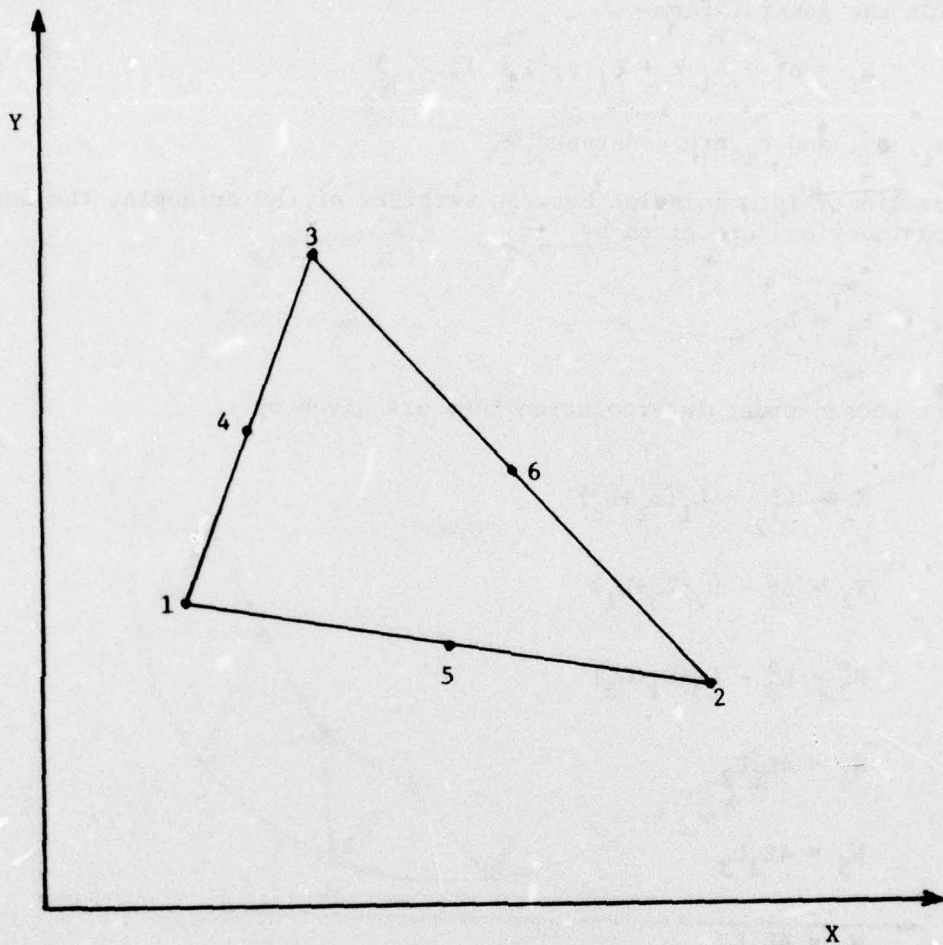


Figure 13. Schematic of Finite Elements Showing Numbering Scheme

$$\frac{\partial I(\phi^{(e)})}{\partial \phi_j} = 0 \quad ; \quad j = 1, 2, 3, \dots, r \quad (68)$$

where $r = 3$ for linear interpolation and $r = 6$ for second-order interpolation.

After performing the indicated differentiations, there is obtained for each element a set of equations of the form

$$[K]\{\phi\} = \{R\} \quad (69)$$

where K_{ij} is an $r \times r$ matrix of influence coefficients relating the nodal variables ϕ_j , which is an $r \times 1$ column vector of nodal values of velocity potential, and R_i is an $r \times 1$ column vector of forcing functions. For this case $r_i = 0$ since $f(x,y,z) = 0$ on the body surface. The k -matrix is obtained by first deriving the element matrix equations and then assembling these elements into a system matrix containing the summation of all of the element contributions to each nodal variable.

The resulting system of equations must be modified to incorporate the nodal boundary conditions as defined in Equation (61). To apply a known value of ϕ at the i th node, the i th system equation is cleared to zero. Then the diagonal entry is set to one and the known value placed on the right-hand side of the system equations in the i th position. This forces the solution of the system to obey the specified boundary conditions at the i th node.

After application of the boundary conditions to the system, the equations are solved by means of a banded Gauss elimination procedure. The band width of the system matrix is highly dependent upon the nodal numbering scheme and is dependent solely upon the maximum difference in nodal numbers within any given element taken over all the elements. It was found that the run time and core storage requirements were significantly reduced with no loss of accuracy by taking into account the banded nature of the system matrix. All of the calculations were performed on an IBM 370/158 computer in single precision mode.

After solving for new values of ϕ , the results were numerically differentiated by means of the interpolation functions. For example,

$$u = \sum_1 \frac{\partial N_1}{\partial x} \phi_1 \quad (70)$$

then the resulting velocities are used in Equation (56) to obtain new values of density at every point. The process was then repeated until convergence was attained.

After the velocities were obtained from the final iteration, the pressure coefficients were obtained from Equation (57)

RESULTS AND CONCLUSIONS

For the case of the 6-percent-thick circular arc airfoil at $M_\infty = 0.707$, the results are shown in Figure 14. Figure 14(A) shows the results for the second-order interpolation functions. The first-order solution appears to be very smooth and follows the experimental trends well even though the finite element grid is quite coarse. It would be expected that this solution would approach the true solution asymptotically as the grid is refined. This, of course, would require a much greater computer core and time.

An alternate method for improving the accuracy of the solution is to use second-order interpolation functions. This technique was implemented with the results shown on Figure 14(B).

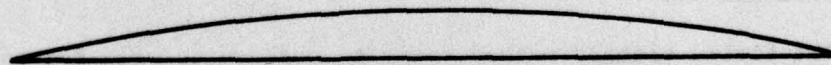
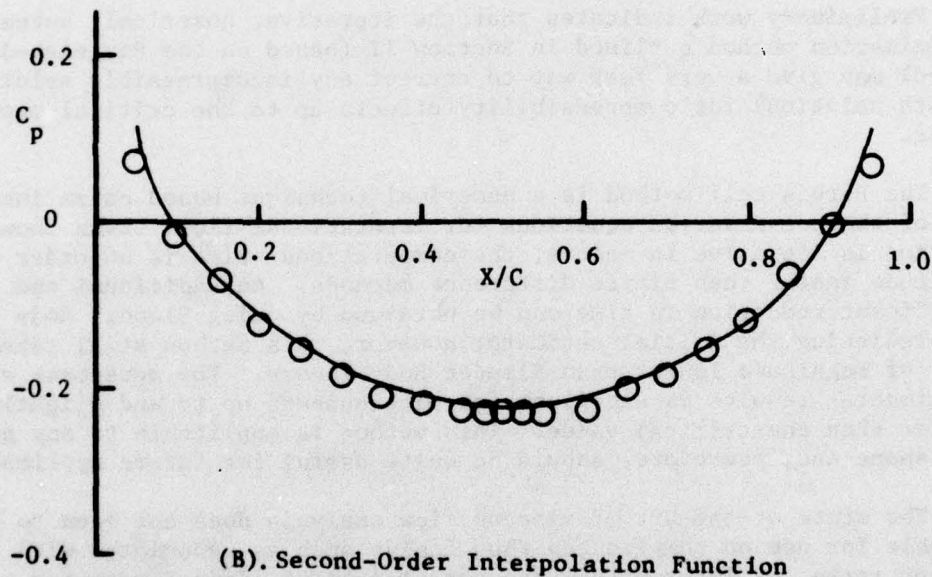
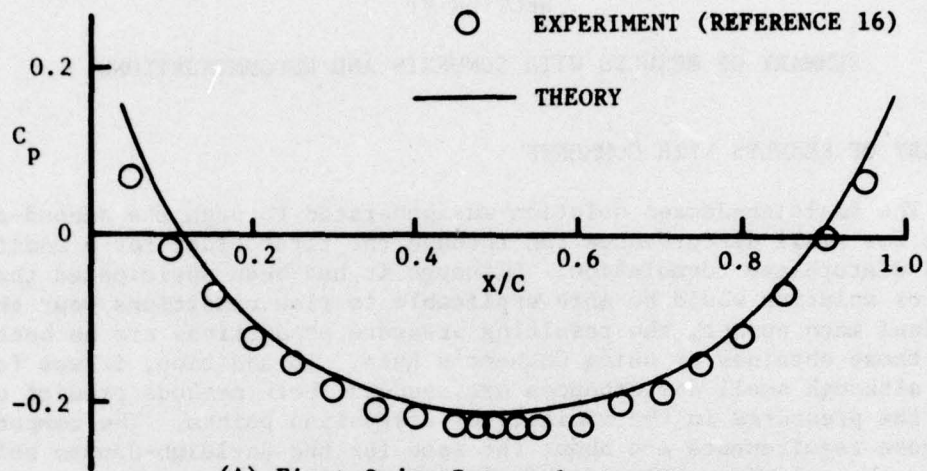


Figure 14. Comparison of the Pressure Distribution for a 6-Percent Parabolic Arc Airfoil Computed by the Finite Elements Method with Experimental Results, $M_\infty = 0.707$

SECTION VI

SUMMARY OF RESULTS WITH COMMENTS AND RECOMMENDATIONS

SUMMARY OF RESULTS WITH COMMENTS

The Rayleigh-Janzen solution was generated through the second-order terms for small disturbances and through the first order for a modified small disturbance formulation. Although it had been anticipated that this type of solution would be more applicable to flow conditions near the critical mach number, the resulting pressure predictions are no better than those obtained by using Gothert's Rule. In addition, it was found that although small disturbances are assumed, both methods predict quite well the pressures in the vicinity of stagnation points. The computer time and core requirements are about the same for the Rayleigh-Janzen solutions as for the solutions using Gothert's Rule, approximately three to five seconds on a CDC 6600 computer.

Preliminary work indicates that the iterative, numerical, successive approximation method outlined in Section II (based on the Rayleigh-Janzen method) may give a very fast way to correct any incompressible solution (zeroth solution) for compressibility effects up to the critical mach number.

The Purvis cell method is a numerical technique based on an integral form of the conservation equations for irrotational flow. Even though this solution is iterative in nature, the computational time is an order of magnitude faster than finite difference methods. An additional and significant reduction in time can be obtained by using Slender Body Theory for predicting the initial estimate; however, this method still takes an order of magnitude longer than Slender Body Theory. The agreement with experimental results is excellent for mach numbers up to and slightly greater than the critical value. This method is applicable to any general body shape and, therefore, should be quite useful for future applications.

The state-of-the-art of viscous flow analysis does not seem to be suitable for use on complicated flow fields such as associated with triple ejector racks, at least within the constraints of limited computer core and computational time.

The finite element method seems to work quite well for potential and some viscous, incompressible flow cases. The application required for mutual interference - compressible, viscous flow, however, has not been successfully formulated.

RECOMMENDATIONS

Several approaches investigated in this work warrant additional study as suggested below:

1. The successive numerical approximation outlined in Section II should be investigated. This technique could be used to correct any incompressible flow solution for compressibility effects.
2. The Purvis cell method should be expanded to include the general three-dimensional problem. Further, it is recommended that a coordinate transformation to rectangular arrays be considered in order to simplify the utilization of this method for arbitrary curved bodies.
3. The potential flow solution should be modified so as to include shock jump effects.

It should be noted that, although the Purvis method takes an order of magnitude longer computer time than the Rayleigh-Janzen or Gothert solutions, the velocities on the body surface are computed as part of the solution. Thus, the complete pressure distribution is available as part of the solution. On the other hand, the times quoted for the Rayleigh-Janzen and Gothert solutions are for the basic solution giving the strength distribution of the source singularities. When these basic solutions are used to compute the complete body pressure distribution, the computational times are the same order of magnitude as for the Purvis method.

APPENDIX A

RAYLEIGH-JANZEN SOLUTION FOR SLENDER BODIES

The velocity potential equation can be written in a form useful in this study to yield

$$a^2 \nabla^2 \phi = - \left(\frac{1}{\gamma-1} \right) \nabla \phi \cdot \nabla a \quad (\text{A-1})$$

where

$$a^2 = a_\infty^2 \left[1 + \left(\frac{\gamma-1}{2} \right) M_\infty^2 (1 - \nabla \phi \cdot \nabla \phi) \right] \quad (\text{A-2})$$

Expanding Equation (A-1) in terms of the nondimensional, perturbation velocity potential yields

$$\begin{aligned} & \left[1 - \left(\frac{\gamma-1}{2} \right) M_\infty^2 (2\phi_x + \phi_x^2 + \phi_y^2 + \phi_z^2) \right] \nabla^2 \phi = \\ & \frac{M_\infty^2}{2} \left[(1 + \phi_x) \frac{\partial}{\partial x} + \phi_y \frac{\partial}{\partial y} + \phi_z \frac{\partial}{\partial z} \right] [2\phi_x + \phi_x^2 + \phi_y^2 + \phi_z^2] \end{aligned} \quad (\text{A-3})$$

Using $\epsilon = M_\infty^2$ as the perturbation parameter, an assumed series solution of the form

$$\begin{aligned} \phi(x, y, z; \epsilon) = & \phi^{(0)}(x, y, z) + \epsilon \phi^{(1)}(x, y, z) + \\ & + \epsilon^2 \phi^{(2)}(x, y, z) + \dots \end{aligned} \quad (\text{A-4})$$

will be considered as follows.

The assumed solution can be substituted into Equation (A-3) and, in principle, each successive order of magnitude term can be solved. For small perturbations, however, Equation (A-3) can be simplified by neglecting velocity squared terms in comparison to first-order terms and Equation (A-3) reduces to

$$[1 - (\gamma-1) M_\infty^2 \phi_x] \nabla^2 \phi = M_\infty^2 \left[(\phi_x + 1) \frac{\partial}{\partial x} + \phi_y \frac{\partial}{\partial y} + \phi_z \frac{\partial}{\partial z} \right] \phi_x \quad (\text{A-5})$$

The right-hand side of Equation (A-5) can now be rewritten into the equivalent form given by Equation (A-6)

$$[1 - (\gamma-1) M_\infty^2 \phi_x] \nabla^2 \phi = M_\infty^2 \frac{\partial}{\partial x} \left[\phi_x + \frac{\phi_x^2 + \phi_y^2 + \phi_z^2}{2} \right] \quad (\text{A-6})$$

Again neglecting second-order velocity terms in comparison to the first-order terms yields

$$[1 - (\gamma-1) M_\infty^2 \phi_x] \nabla^2 \phi = M_\infty^2 \phi_{xx} \quad (\text{A-7})$$

The body boundary conditions for axisymmetric bodies at zero angle of attack can be expressed as

$$\phi_y \cos \theta + \phi_z \sin \theta = (1 + \phi_x) \frac{dr}{dx} \Big|_{\text{body}} \quad (\text{A-8})$$

Substituting Equation (A-4) into Equations (A-7) and (A-8), and equating terms in powers of ϵ gives the first three orders of magnitude equations as follows:

ZEROth ORDER

$$\nabla^2 \phi^{(0)} = 0 \quad (\text{A-9a})$$

$$\phi_y^{(0)} \cos \theta + \phi_z^{(0)} \sin \theta = (1 + \phi_x^{(0)}) \frac{dr}{dx} \Big|_{\text{body}} \quad (\text{A-9b})$$

FIRST ORDER

$$\nabla^2 \phi^{(1)} = \phi_{xx}^{(0)} \quad (\text{A-10a})$$

$$\phi_y^{(1)} \cos \theta + \phi_z^{(1)} \sin \theta = \phi_x^{(1)} \frac{dr}{dx} \Big|_{\text{body}} \quad (\text{A-10b})$$

SECOND ORDER

$$\nabla^2 \phi^{(2)} = \phi_x^{(0)} \phi_{xx}^{(0)} + \phi_{xx}^{(1)} \quad (\text{A-11a})$$

$$\phi_y^{(2)} \cos \theta + \phi_z^{(2)} \sin \theta = \phi_x^{(2)} \frac{dr}{dx} \Big|_{\text{body}} \quad (\text{A-11b})$$

SOLUTION FOR AXISYMMETRIC BODIES ($\alpha=0$)

For axisymmetric bodies at zero angle of attack, the solution, including the image system for mutual interference, can be expressed as the sum of the source singularities as given by Equation (A-12) for the zeroth solution.

$$\phi^{(0)} = \sum_i \frac{-C_{o_i}}{R_i} \quad (\text{A-12})$$

where

$$R_i = \sqrt{(x-x_i)^2 + (y-y_i)^2 + (z-z_i)^2} \quad (\text{A-13})$$

and the source strengths, C_{o_i} , are determined so as to satisfy the body boundary conditions.

The first-order solution which satisfies Equation (A-10) can be expressed as

$$\phi^{(1)} = \sum_j \frac{-C_{1_j}}{R_j} + \frac{1}{2} \sum_i \frac{C_{o_i} (x-x_i)^2}{R_i^3} \quad (\text{A-14})$$

where the source strengths, C_{1_j} , are determined by satisfying the first-order boundary conditions.

After using Equations (A-12) and (A-14) in (A-11), the second-order solution can be found to be

$$\begin{aligned} \phi^{(2)} = & \sum_k \frac{-C_{2_k}}{R_k} + \frac{13}{12} \sum_i \frac{C_{o_i}}{R_i} + \frac{7}{6} \sum_j \frac{C_{1_j}}{R_j} - \frac{1}{12} \sum_i \frac{C_{o_i} (x-x_i)^2}{R_i^3} \\ & + \frac{1}{6} \sum_j \frac{C_{1_j} (x-x_j)^2}{R_j^3} + \frac{3}{8} \sum_i \frac{C_{o_i} (x-x_i)^4}{R_i^5} \\ & + (\gamma-1) \sum_i \frac{C_{o_i} (x-x_i)}{R_i^3} - \sum_i \frac{1}{2} \frac{C_{o_i} (x-x_i)^2}{R_i^3} \end{aligned} \quad (\text{A-15})$$

The source strengths, C_{2_k} , must be found so as to satisfy the second-order boundary conditions.

The constants, C_{1j} and C_{2k} , are the source singularity strengths for the complimentary solutions of Equations (A-10) and (A-11), respectively. It is possible, however, that in addition to (or rather than) the sources, doublet singularities may be required in order to satisfy the boundary conditions. If that is the case, Equations (A-14) and (A-15) will require terms such as given by Equation (A-16).

$$\phi \Big|_{\text{doublets}} = \sum_{\ell} \frac{\mu_{\ell} (x-x_{\ell})}{R_{\ell}^3} + \sum_{m} \frac{\mu_m (y-y_m)}{R_m^3} + \sum_n \frac{\mu_n (z-z_n)}{R_n^3} \quad (\text{A-16})$$

The three terms in Equation (A-16) are for doublets with their axis along the x-, y-, and z-directions, respectively.

AXISYMMETRIC BODY AT ANGLE OF ATTACK, α

For axisymmetric bodies at angle of attack, the solution can be expressed as the sum of source singularities plus the sum of doublet singularities which are needed in order to satisfy the body boundary conditions due to the cross-flow. In this case, the body boundary conditions can be expressed by Equation (A-17).

$$\phi_y \cos \theta + (\phi_z + \sin \alpha) \sin \theta = (\phi_x + \cos \alpha) \frac{dr}{dx} \Big|_{\text{body}} \quad (\text{A-17})$$

The order of magnitude boundary conditions obtained by substituting Equation (A-4) into Equation (A-17) becomes, for the first three terms,

$$\phi_y^{(0)} \cos \theta + (\phi_z^{(0)} + \sin \alpha) \sin \theta = (\phi_x^{(0)} + \cos \alpha) \frac{dr}{dx} \Big|_{\text{body}} \quad (\text{A-18})$$

$$\phi_y^{(1)} \cos \theta + \phi_z^{(1)} \sin \theta = \phi_x^{(1)} \frac{dr}{dx} \Big|_{\text{body}} \quad (\text{A-19})$$

$$\phi_y^{(2)} \cos \theta + \phi_z^{(2)} \sin \theta = \phi_x^{(2)} \frac{dr}{dx} \Big|_{\text{body}} \quad (\text{A-20})$$

The zeroth solution for this case can be expressed as Equation (A-11)

$$\phi^{(0)} = \sum_i \frac{-C_{0i}}{R_i} + \sum_j \frac{\mu_{0j} (z-z_j)}{R_j} \quad (\text{A-21})$$

where the singularity strengths must be found so as to satisfy Equation (A-18). Note, however, that the zeroth order solutions can be obtained by solving the axisymmetric-flow problem and the cross-flow problem. Splitting

the body boundary conditions into the axial and cross-flow components yields for the axial flow problem,

$$\phi_y^{(0)} \cos \theta + \phi_z^{(0)} \sin \theta = (\phi_x^{(0)} + \cos \alpha) \frac{dr}{dx} \Big|_{\text{body}} \quad (\text{A-22})$$

where only the source singularities are considered.

For the cross-flow, the body boundary conditions are expressed by Equation (A-23) where only the doublet singularities are considered.

$$\phi_y^{(0)} \cos \theta + (\phi_z^{(0)} + \sin \alpha) \sin \theta = \phi_x^{(0)} \frac{dr}{dx} \Big|_{\text{body}} \quad (\text{A-23})$$

The axial-flow solution remains the same as that found by Equation (A-11) except that the boundary condition equation must be corrected by using the axial component of the free-stream speed as given by Equation (A-22).

The cross-flow solution is now given by Equation (A-24) where Equation (A-23) is used to determine the doublet singularities.

$$\phi^{(0)} \Big|_{\text{cross-flow}} = \sum_j \frac{\mu_{0j} (z-z_{1j})}{R_j^3} \quad (\text{A-24})$$

The first-order equations can also be solved by considering the axial-flow and the cross-flow solutions. As in the zeroth solution, the axial-flow solution is the same form as given by Equation (A-14).

The governing equations for the cross-flow problem are found by substituting Equation (A-24) into Equation (A-10a) and yields

$$\phi^{(1)} \Big|_{\text{cross-flow}} = \sum_k \frac{\mu_{1k} (z-z_k)}{R_k^3} + \frac{3}{2} \sum_j \frac{\mu_{0j} (z-z_j)^2}{R_j^5} \quad (\text{A-26})$$

The second-order equation [see Equation (A-11a)] contains nonlinear terms and, therefore, cannot be solved by separating the axial-flow and cross-flow solutions. Hence, the governing equations for this case is

$$\nabla^2 \phi^{(2)} = (\gamma-1) \left(\sum_i \frac{C_{o_i} (x-x_i)}{R_i^3} + \sum_j \frac{3\mu_{o_j} (z-z_j)(x-x_j)}{R_j^5} \right) x$$

$$\left(\sum_i C_{o_i} \left[\frac{1}{R_i^3} - \frac{3(x-x_i)^2}{R_i^5} \right] + \sum_j 3\mu_{o_j} (z-z_j) \left[\frac{1}{R_j^5} - \frac{5(x-x_j)^2}{R_j^7} \right] \right)$$

$$+ \sum_i \left[\frac{C_{1_i}}{R_i^3} - \frac{3C_{1_i} (x-x_i)^2}{R_i^5} \right] + \frac{1}{2} \sum_i \left[\frac{2C_{o_i}}{R_i^3} - \frac{15C_{o_i} (x-x_i)^2}{R_i^5} + \frac{15C_{o_i} (x-x_i)^4}{R_i^7} \right]$$

$$+ \sum_k \left[\frac{2\mu_{1_k} (z-z_k)}{R_k^3} - \frac{15\mu_{1_k} (z-z_k)(x-x_k)^2}{R_k^5} + \frac{15\mu_{1_k} (z-z_k)(x-x_k)^4}{R_k^7} \right]$$

$$+ \frac{3}{2} \sum_j \mu_{o_j} (z-z_j) \left[\frac{2}{R_j^5} - \frac{25(x-x_j)^2}{R_j^7} + \frac{35(x-x_j)^4}{R_j^9} \right]$$

(A-28)

The general solution for the second-order term can be expressed as

$$\begin{aligned}
 \phi^{(2)} = & \sum_i \frac{-C_{2i}}{R_i} + \sum_j \frac{\mu_{2j} (z-z_j)}{R_j^3} \\
 & + (\gamma-1) \left(\sum_i \frac{C_{0i} (x-x_i)}{R_i^3} + \sum_j \frac{3\mu_{0j} (z-z_j)(x-x_j)}{R_j^5} \right) x \\
 & \left(\sum_i \frac{\frac{1}{2}C_{0i} (x-x_i)^2}{R_i^3} + \frac{3}{2} \sum_j \frac{\mu_{0j} (x-x_j)^2(z-z_j)}{R_j^5} \right) \\
 & + \frac{1}{2} \sum_i \frac{C_{1i} (x-x_i)^2}{R_i^3} + \frac{1}{2} \left[\sum_i \frac{C_{0i} (x-x_i)^2}{R_i^3} - \frac{3}{4} \sum_i \frac{C_{0i} (x-x_i)^4}{R_i^5} \right] \\
 & + \sum_k \left[\frac{2\mu_{1k} (z-z_k)(x-x_k)^2}{R_k^3} - \frac{1}{2} \mu_{1k} \frac{(z-z_k)(x-x_k)}{R_k^5} \right] \\
 & + \frac{3}{2} \sum_j \left[\frac{\mu_{0j} (z-z_j)(x-x_j)^4}{R_j^5} - \frac{5}{4} \frac{\mu_{0j} (z-z_j)(x-x_j)^4}{R_j^7} \right]
 \end{aligned} \tag{A-28}$$

APPENDIX B

MODIFIED SLENDER BODY SOLUTION

The governing partial differential equation which properly accounts for stagnation conditions, small velocity perturbations away from stagnation points, and conditions up to the critical mach number [given in Section II as Equation (20)] is given here as Equation (B-1).

$$\nabla^2 \phi = \left[\frac{\partial}{\partial x} + \nabla \phi \cdot \nabla \right] \left[M_\infty^2 \phi_x + \left(\frac{\gamma-1}{2} \right) M_\infty^4 \phi_x^2 \right] \quad (\text{B-1})$$

Equation (B-1) in a slightly more convenient form becomes

$$\nabla^2 \phi = M_\infty^2 [1 + (\gamma-1) M_\infty^2 \phi_x] [\phi_{xx} + \nabla \phi \cdot \nabla \phi_x] \quad (\text{B-2})$$

The solution of Equation (B-2) can now be generated by the Rayleigh-Janzen method as follows:

Assuming the solution

$$\phi = \phi^{(0)} + M_\infty^2 \phi^{(1)} + M_\infty^4 \phi^{(2)} + \dots \quad (\text{B-3})$$

yields

$$(0) ; \nabla^2 \phi^{(0)} = 0 \quad (\text{B-4a})$$

$$(1) ; \nabla^2 \phi^{(1)} = \phi_{xx}^{(0)} + \nabla \phi^{(0)} \cdot \nabla \phi_x^{(0)} \quad (\text{B-4b})$$

$$(2) ; \nabla^2 \phi^{(2)} = \phi_{xx}^{(1)} + \nabla \phi^{(0)} \cdot \nabla \phi_x^{(1)} + \nabla \phi^{(1)} \cdot \nabla \phi_x^{(0)} \\ + (\gamma-1) \phi_x^{(0)} \nabla^2 \phi^{(1)} \quad (\text{B-4c})$$

⋮

The body boundary conditions are:

$$(0) ; \phi_y^{(0)} \cos \theta + (\phi_z^{(0)} + \sin \alpha) \sin \theta = (\phi_x^{(0)} + \cos \alpha) \left(\frac{dr}{dx}\right)_{\text{body}} \quad (\text{B-5a})$$

$$(1) ; \phi_y^{(1)} \cos \theta + \phi_z^{(1)} \sin \theta = \phi_x^{(1)} \left(\frac{dr}{dx}\right)_{\text{body}} \quad (\text{B-5b})$$

$$(2) ; \phi_y^{(2)} \cos \theta + \phi_z^{(2)} \sin \theta = \phi_x^{(2)} \left(\frac{dr}{dx}\right)_{\text{body}} \quad (\text{B5c})$$

⋮
⋮
⋮

The zeroth solution expressed in the usual manner as the sum of sources and doublet yields

$$\phi^{(0)} = \sum_i (\phi_{S_i}^{(0)}) + \sum_j (\phi_{D_j}^{(0)}) \quad (\text{B-6})$$

For the first-order solution, we need to satisfy the equation

$$\nabla^2 \phi^{(1)} = \phi_{xx}^{(0)} + \nabla \phi^{(0)} \cdot \nabla \phi_x^{(0)} \quad (\text{B-7})$$

Consider first the following expression

$$\phi = (\phi^{(0)} \phi_x^{(0)}) \quad (\text{B-8})$$

which can be expanded to give

$$\nabla^2 (\phi^{(0)} \phi_x^{(0)}) = \phi^{(0)} \nabla^2 \phi_x^{(0)} + \phi_x^{(0)} \nabla^2 \phi^{(0)} + 2 \nabla \phi^{(0)} \cdot \nabla \phi_x^{(0)} \quad (\text{B-9})$$

But

$$\nabla^2 \phi_x^{(0)} = \nabla^2 \phi^{(0)} = 0 \quad (\text{B-10})$$

Therefore

$$\nabla^2 (\phi^{(0)} \phi_x^{(0)}) = 2 \nabla \phi^{(0)} \cdot \nabla \phi_x^{(0)} \quad (\text{B-11})$$

For the $\phi_{xx}^{(0)}$ - term, it can be shown that

$$\nabla^2 \left[-\frac{1}{2} \sum_i \frac{(x-x_i)^2}{R_i^2} \phi_{s_i}^{(0)} - \frac{3}{2} \sum_j \frac{(x-x_j)^2}{R_j^2} \phi_{D_j}^{(0)} \right] = \phi_{xx}^{(0)} \quad (\text{B-12})$$

Thus, the particular solution for sources and doublets can be written as

$$[\phi^{(1)}]_P = -\frac{1}{2} \sum_i \frac{(x-x_i)^2}{R_i^2} \phi_{s_i}^{(0)} - \frac{3}{2} \sum_j \frac{(x-x_j)^2}{R_j^2} \phi_{D_j}^{(0)} + \frac{1}{2} \sum \phi^{(0)} \phi_x^{(0)} \quad (\text{B-13})$$

where the zeroth solution $\phi^{(0)}$ is

$$\phi^{(0)} = \sum_i \phi_{s_i}^{(0)} + \sum_j \phi_{D_j}^{(0)} \quad (\text{B-14})$$

and

$$\phi_x^{(0)} = \sum_i \phi_{x s_i}^{(0)} + \sum_j \phi_{x D_j}^{(0)} \quad (\text{B-15})$$

The complementary solution can be written as

$$[\phi^{(1)}]_C = \sum_i \phi_{s_i}^{(1)} + \sum_j \phi_{D_j}^{(1)} \quad (\text{B-16})$$

and the first-order solution becomes

$$\phi^{(1)} = [\phi^{(1)}]_C + [\phi^{(1)}]_P \quad (\text{B-17})$$

REFERENCES

1. Martin, F. W., "Mutual Aerodynamic Interference Effects for Multiple Bodies by the Cross-Flow Corrections Method," AFATL-TR-71-69, Air Force Armament Laboratory, Eglin Air Force Base, Florida, June 1971.
2. Martin, F. W., "Cross-Flow Corrected Axisymmetric Solution for Multiple Body Interference," AFATL-TR-71-109, Air Force Armament Laboratory, Eglin Air Force Base, Florida, August 1971.
3. Martin, F. W., Smith, C. J., and Saunders, G. H., "Mutual Aerodynamic Interference Effects for Two Axisymmetric Bodies," AFATL-TR-73-161, Air Force Armament Laboratory, Eglin Air Force Base, Florida, August 1973.
4. Walkley, K. B., and Martin, F. W., "Aerodynamic Interference of Wing-Pylon-Body Combinations at Low Subsonic Speeds," AFATL-TR-73-162, Air Force Armament Laboratory, Eglin Air Force Base, Florida, August 1973.
5. May, R. C., and Martin, F. W., "Effects of Triple Ejector Rack Geometry on the Pressure Distribution of the M-117 Bomb," AFATL-TR-74-21, Air Force Armament Laboratory, Eglin Air Force Base, Florida, August 1974.
6. Martin, F. W., "Image System Solution for Mutual Aerodynamic Interference," Presented as Paper No. 35, Aircraft/Stores Compatibility Symposium, Wood Lake Inn, Sacramento, California, September 1973.
7. Martin, F. W., and Walkley, K. B., "Image System Solution for Store Aerodynamics with Interference - Part II," Journal of Aircraft, Vol. 12, No. 3, March 1975, pp. 156-161.
8. Martin, F. W., Saunders, G. H., and Smith, C. J., "Image System Solution for Store Aerodynamics with Interference - Part I," Vol. 12, No. 3, March 1975, pp. 151-155.
9. Martin, F. W., Saunders, G. H., and Cutchins, M. A., "Mutual Aerodynamic Interference Effects for Multiple Bodies of Revolution and Distorted Bodies of Revolution," AFATL-TR-76-47, Air Force Armament Laboratory, Eglin Air Force Base, Florida, April 1976.
10. Burkhalter, J. E., and Martin, F. W., "Aerodynamic Interference of Two Axisymmetric Stores at Low Supersonic Speeds," Final Report, Air Force Armament Laboratory, Eglin Air Force Base, Florida, September 1976.
11. "The Dynamics and Thermodynamics of Compressible Fluid Flow," pp. 336, 365-367, 317, by Ascher H. Shapiro, The Ronald Press Company, NY, 1953.

REFERENCES (CONCLUDED)

12. "Perturbation Methods in Fluid Mechanics," Milton Van Dyke, Academic Press, 1964.
13. Mattasits, G. R., "Aerodynamic Interference Effects on Various Weapon Shapes in the Flow Field of a Transonic Wing Configuration at Mach Numbers from 0.5 to 1.3," AFATL-TR-75-88 (AEDC-TR-75-92), July 1975, Prepared for Air Force Armament Laboratory (AFATL/DLJC), Eglin Air Force Base, Florida.
14. Roache, Patrick J., "Computational Fluid Dynamics," Hermosa Publishers, 1972.
15. Zienkiewicz, O. C., "The Finite Element Method in Engineering Science," McGraw-Hill, 1971.
16. Murman, E. M., and Cole, J. D., "Calculation of Plane Steady Transonic Flows," AIAA Journal, Vol. 9, No. 1, January 1971.
17. South, J. C., and Jameson, A., "Relaxation Solutions for Inviscid Axisymmetric Transonic Flow over Blunt or Pointed Bodies," Proceedings: AIAA Computational Fluid Dynamics Conference, July 1973.
18. Sasman, P. K., and Cresci, R. J., "Compressible Turbulent Boundary Layer with Pressure Gradient and Heat Transfer," AIAA Journal, Vol. 4, No. 1, January 1966.
19. Martin, Harold C., and Carey, Graham F., "Introduction to Finite Element Analysis, Theory and Application," McGraw-Hill Book Company, New York, 1973.
20. Huebner, Kenneth H., "The Finite Element Method for Engineers," John Wiley and Sons, Inc., New York, 1975.
21. "Symposium on Finite Elements in Fluid Flow," University of Alabama Press, Huntsville, Alabama, 1971.

INITIAL DISTRIBUTION

Hq USAF/RDQRM	2	USAF/XOOE	1
Hq USAF/SAMI	1	AFFDL/FGC	1
Hq USAF/XOXFM	1	AFATL/DLODR	1
AFIS/INTA	1	NSWC/Tech Lib & Info Svs/Dahlgren	1
AFSC/DLCA	1	TAC/INA	1
AFSC/IGFG	1	ASD/XRP	1
AFSC/SDZA	1		
ASD/ENFEA	1		
FTD/PDXA-2	1		
AFWL/NSC	1		
AFEWC/SUR	4		
AUL (AU/LSE-70-239)	2		
DDC	2		
NRSLC/MMIRBD	1		
Ogden ALC/MMWM	2		
TAC/DRA	1		
6510 ABG/SSD	1		
Hq USAFE/DOA	1		
Hq USAFE/DOQ	1		
Hq PACAF/LGWSE	1		
Hq PACAF/DOO	1		
Redstone Sci Info Cen/Doc Sec	2		
NRL/Code 2627	1		
Navair Sys Comd/Code 530C	1		
Navair Sys Comd/Tech Lib/AIR-954	1		
NSWC/Tech Lib & Info Svs/White Oak	2		
Naval Air Test Center/CT-176 TID/ Tech Pubs	2		
USNWC/Code 533	1		
Sandia Lab/Tech Lib-Div 3141	1		
The Rand Corp/Library-D	1		
TACTEC/Battelle Columbus Lab	1		
TAWC/TRADOCLO	1		
ADTC/SES	1		
AFATL/DL	1		
AFATL/DLODL	9		
AFATL/DLJ	1		
AFATL/DLJC	8		
Naval Ship R&D Cen/Code 166/Acft Div	1		
Naval Wpns Eval Fac/Weapons Dept	1		
USNWC/Code 4063	1		
AFATL/DLJA	1		
USAFE/LGWM	1		
AFSC/SDTA	1		
AFIT/LD	1		
ASD/ENESS	1		